AWARD NUMBER: W81XWH-18-1-0690

TITLE: Therapeutic Targeting of Neuroendocrine Prostate Cancer

PRINCIPAL INVESTIGATOR: Eva Corey

CONTRACTING ORGANIZATION: University of Washington, Seattle, WA

REPORT DATE: December 2023

TYPE OF REPORT: Final

PREPARED FOR: U.S. Army Medical Research and Development Command
Fort Detrick, Maryland, 21702-5012

DISTRIBUTION STATEMENT: Approved for Public Release;
Distribution Unlimited

REPORT DOCUMENTATION PAGE

Form Approved
OMB No. 0704-0188

1. REPORT DATE	2. REPORT TYPE	3. DATES COVERED
December 2023	FINAL	01Sep2018-31Aug2023

4. TITLE AND SUBTITLE

Therapeutic Targeting of Neuroendocrine Prostate Cancer

5a. CONTRACT NUMBER
W81XWH-18-1-0690

5b. GRANT NUMBER
PC170350P2

5c. PROGRAM ELEMENT NUMBER

6. AUTHOR(S)
Eva Corey

E-Mail: ecorey@uw.edu

5d. PROJECT NUMBER

5e. TASK NUMBER

5f. WORK UNIT NUMBER

7. PERFORMING ORGANIZATION NAME(S) AND ADDRESS(ES)

University of Washington
4333 Brooklyn Ave
Seattle WA 98195-9472

8. PERFORMING ORGANIZATION REPORT NUMBER

9. SPONSORING / MONITORING AGENCY NAME(S) AND ADDRESS(ES)

U.S. Army Medical Research and Development Command
Fort Detrick, Maryland 21702-5012

10. SPONSOR/MONITOR'S ACRONYM(S)

11. SPONSOR/MONITOR'S REPORT NUMBER(S)

12. DISTRIBUTION / AVAILABILITY STATEMENT

Approved for Public Release; Distribution Unlimited

13. SUPPLEMENTARY NOTES

14. ABSTRACT

Increased incidence of treatment induced neuroendocrine prostate cancer (NEPC) is particularly alarming as this diagnosis is associated with poor prognosis and decades of cytotoxic chemotherapy as the only treatment option. We previously identified neuronal transcription factor BRN2 as a potent driver of neuroendocrine differentiation and an attractive target in NEPC. Our goal is to Evaluate the mechanism by which BRN2 alters chromatin architecture to support neuroendocrine lineage reprogramming. To facilitate any future clinical use of a BRN2 inhibitor in PCa, the project described herein aimed to identify a biomarker of BRN2positive (BRN2+) NEPC that can be readily detected in serum from patients. This would enable longitudinal monitoring of patients for development of BRN2+ NEPC, similarly to how prostate-specific antigen (PSA) levels are currently monitored to gauge PCa progression, and thus potentially provide the means for early detection of PCa patients who may benefit from a BRN2 inhibitor. This report documents progress made towards this aim. Using unbiased approach by combining ChIPseq, RNAseq and secreted protein analysis, we identified Neuronal pentraxin 1 (NPTX1) as a promising biomarker and validated that it can be detected in serum from PCa patients.

15. SUBJECT TERMS
None listed.

16. SECURITY CLASSIFICATION OF:			17. LIMITATION OF ABSTRACT	18. NUMBER OF PAGES	19a. NAME OF RESPONSIBLE PERSON
a. REPORT	b. ABSTRACT	c. THIS PAGE			USAMRDC
Unclassified	Unclassified	Unclassified	Unclassified	42	19b. TELEPHONE NUMBER *(include area code)*

Table of Contents

Introduction

Lineage plasticity has been postulated to contribute to the failure of targeted- and immuno-therapies[2, 3]. In prostate cancer (PCa), the discovery that metastatic castration-resistant PCa (CRPC), classified as adenocarcinoma (CRPC-Ad), remains fueled by the androgen receptor (AR) has ushered the development of potent androgen receptor pathway inhibitors (ARPIs). This includes enzalutamide (ENZ)[4], abiraterone (ABI)[5], and Apalutamide (APA)[6] which have undoubtedly benefited the survival of patients with advanced disease. However, a subset of patients (~20%) relapse with tumours that are no longer dependent on androgen receptor activity and, instead, exhibit activation of alternative lineage programs, including stem cell and neuronal pathways[7, 8]. These tumours, termed treatment-emergent neuroendocrine PCa (NEPC), are particularly aggressive and, due to no targeted therapeutic strategies, the prognosis is poor with an overall survival of 1 year. Managing NEPC patients and developing novel therapeutic strategies have so far proven challenging. Our group and others point to an epigenetic basis for treatment-emergent NEPC[9-13]. However, there is still much to be known about the fundamental cellular and molecular interactions that bias lineage specification following ARPIs.

Using innovative PCa models coupled with state-of-the-art technologies, a series of ENZ-resistant (ENZR) including t-NEPC[9, 10, 14] and a large cohort of PCa patient-derived xenografts[8].Targeted treatments for this deadly disease are desperately needed. We previously identified that the neuronal transcription factor (TF) BRN2 (POU3F2) is a crucial regulator of NEPC [14] and is highly expressed in NEPC tumors[7, 14]. Moreover, BRN2 is significantly upregulated in small cell lung (SCLC) and bladder cancers[15, 16]. Targeting BRN2 in SCLC models reduced cell proliferation and neuroendocrine marker expression[17]. As a key developmental TF for neuronal cell lineage in the hypothalamus[18], BRN2 has been extensively studied for its ability to induce neurons in both mouse and human lineages in co-operation with other TF like ASCL1 and SOX2[19, 20]. Furthermore, BRN2's expression is paramount for maintaining the tumor-initiating potential of glioblastoma cells[21] and it is a critical driver of invasive and metastatic melanoma[22]. We have since developed a highly specific and potent small molecule BRN2 inhibitor (BRN2i). This project is centered on testing a new paradigm that epigenetic reprogramming, driven by BRN2, represents a molecular "conduit" to aggressive NEPC.

Our research posits that blocking the ability of cells to acquire a plastic phenotype via BRN2 inhibitor may delay/inhibit lineage transformation and extend the durability of clinically beneficial ARPIs and/or treat NEPC.

Keywords

Prostate cancer, neuroendocrine, treatment, BRN2, small molecule inhibitor, ChIP-seq, ATAC-seq, RNA-seq, serum marker, transcription factor, pioneer factor, ELISA

Key Research Accomplishments

- We conducted RNA-seq, ChIP-seq, ATAC-seq on NEPC cell lines following BRN2 inhibition using our lead small molecule inhibitor.

- We generated BRN2 ChIP-seq replicates in our NEPC cell line model to validate our biological observations.

- We performed ATAC-seq on CRPC cell lines following BRN2 overexpression to gain access to both accessible DNA and nucleosome positioning data influenced by BRN2.

- We performed ChIP-seq for histone marks to assess BRN2 influence on the histone map and lineage plastic program in CRPC following BRN2 overexpression.

- We generated a BRN2 signature to assist with patient's identification and segregation.

- We conducted *in vivo* studies to evaluate activity of the lead BRN2 18-94 inhibitor as monotherapy or in combination with carboplatin using PDX models and conducted RNA-seq on the generated tumors.

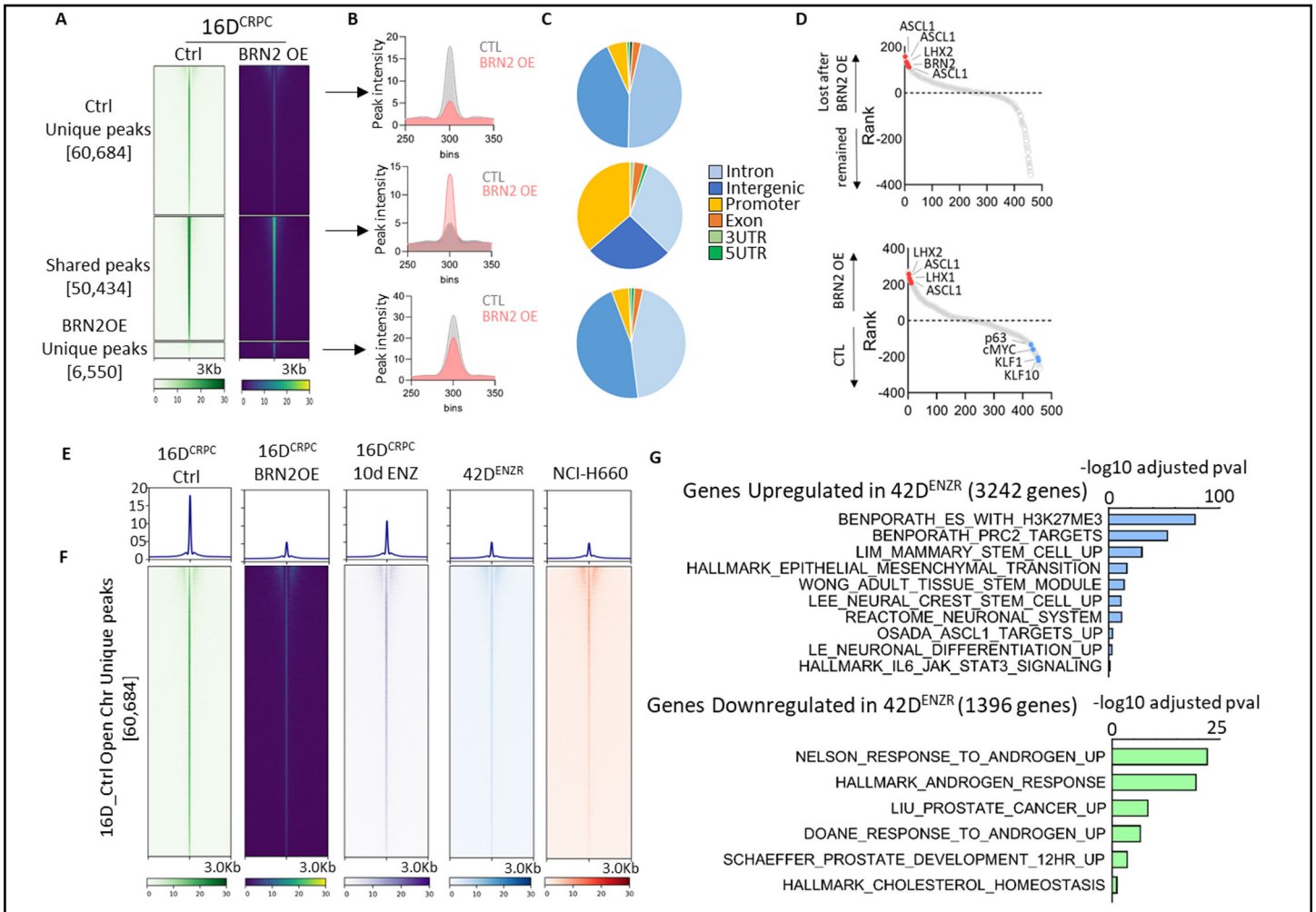

Figure 1: A) Heatmap shows chromatin accessibility in 16D^{CRPC} following overexpression of BRN2 for 72 hours. **B)** Histogram shows peak intensity in regions lost after BRN2 overexpression (top), regions remained accessible (middle), and regions gained following BRN2 overexpression (bottom). **C)** Chromatin accessible annotations to promoter or non-promoter (enhancer) in regions lost after BRN2 overexpression (top), regions remained accessible (middle), and regions gained following BRN2 overexpression (bottom). **D)** Motif analysis comparing regions lost after BRN2 overexpression compared to shared regions (top), and regions gained compared to regions lost after BRN2 following BRN2 overexpression (bottom). Motifs are ranked based on p-value. **E and F)** Histogram and heatmap show lost regions in 16D^{CRPC} following overexpression of BRN2 for 72hours in CRPC cell line following inhibition of androgen receptor (AR) using 10uM enzalutamide for 10 days (10d ENZ) and NEPC cell lines 42D^{ENZR} and NCI-H660. **G)** Gene set enrichment analysis on genes up-regulated in NEPC (42D^{ENZR}) compared to CRPC (16D^{CRPC}) (top) or down-regulated in NEPC (42D^{ENZR}) compared to CRPC (16D^{CRPC}). p-value<0.05.

In order to better characterize the observed BRN2 chromatin remodelling, we focused on NEPC cell line 42D^{ENZR} and conducted ChIP-seq for histone marks for transcriptionally active marks H3K27ac along with H3K27me3 for transcriptional inactivity and mapping them to our ATAC-seq data from 16D^{CRPC} control and following BRN2 overexpression. Loci possessing active histone mark H3K27Ac were higher in shared accessible regions in signal intensity following BRN2 overexpression in CRPC cell line or in NEPC cell line compare to CRPC control. While we observed the active histone mark H3K27Ac in regions lost following BRN2 overexpression in CRPC and in NEPC cell lines, the gained accessible regions lacked any signal. Of note, these regions were depleted from H3K27me3 mark suggestive of an active transcription (Fig. 2).

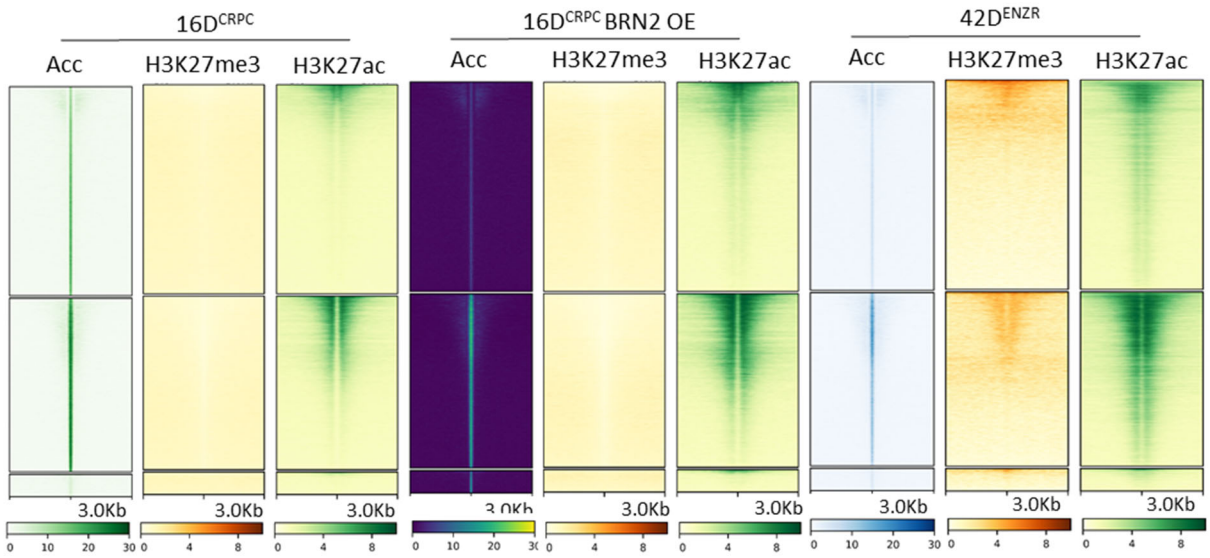

Figure 2: Heatmap shows lost regions in 16D^{CRPC} following overexpression of BRN2 for 72 hours in CRPC cell line and NEPC cell lines 42D^{ENZR} chromatin accessibility overlaid with H3K27me3 and H3K27ac ChIPseq.

To further investigate BRN2's role in epigenetic remodelling resulting in the transformation from adenocarcinoma to NEPC we compared the chromatin accessibility of 16D^{CRPC} following BRN2 overexpression to NEPC cell line 42D^{ENZR} to assess the extent of neuronal differentiation influenced by BRN2. We observed a significant number of regions (40,446 regions) that were shared between 16D^{CRPC} BRN2 overexpressing cells and 42D^{ENZR} (Fig. 3A). One-third of shared accessible regions were annotated to promoters (Fig. 3B), while the accessible regions that were unique to each condition were mostly within enhancers (intron and intergenic) (Fig. 3B). These results suggest that, distal regulatory elements appeared to be most significantly affected by BRN2 presence, while promoters experienced only a few significant alterations in accessibility. Importantly when we compared the genes accessible in 16D^{CRPC} BRN2 overexpressing cells to 42D^{ENZR} we observed 90% overlapped (Fig. 3C), suggesting that the chromatin remodelling reconstructed by BRN2 significantly resembles that of NEPC. Interestingly, pathways enriched in accessible regions mapped to common genes between 16D^{CRPC} BRN2 overexpressing cells and 42D^{ENZR} belonged to plasticity-related pathways (Fig. 4D). Next to better characterize the extend of similarities observed between BRN2-dependent chromatin remodelling and NEPC cell line 42D^{ENZR}, we conducted ChIP-seq for histone marks for transcriptionally active marks H3K27ac along with H3K27me3 for transcriptional inactivity and mapping them to our ATAC-seq data from 16D^{CRPC} following BRN2 overexpression, and overlaid them with histone marks in 42D^{ENZR} (Fig. 3E). Loci possessing active histone mark H3K27Ac were present in both cell lines, although higher in 42D^{ENZR} in signal intensity compared to 16D^{CRPC} following BRN2 overexpression. Suggesting that while BRN2 is remodelling the chromatin accessibility in favour of NEPC phenotype, it also influences the depositing of active histone mark similar to NEPC. While we observed the active histone mark H3K27Ac influenced by BRN2 overexpression, it seems that the deposition of H3K27me3 is not dependent on BRN2, since we did not observe any signal following BRN2 overexpression in regions where H3K27me3 is present in 42D^{ENZR} (Fig. 3F). Moreover, to identify possible co-activators or transcription factors influenced by BRN2 overexpression with a role in NEPC we performed motif enrichment analysis on the regions unique to 16D^{CRPC} BRN2 overexpression, shared regions between 16D^{CRPC} BRN2 overexpression and NEPC, and regions unique to NEPC cell line. We ranked the motifs based on their log10 p-value and observed significant enrichment of CTCF, BORIS (or CTCFL is a paralog of CTCF) and FOX family motifs in each of regions (Fig. 3G).

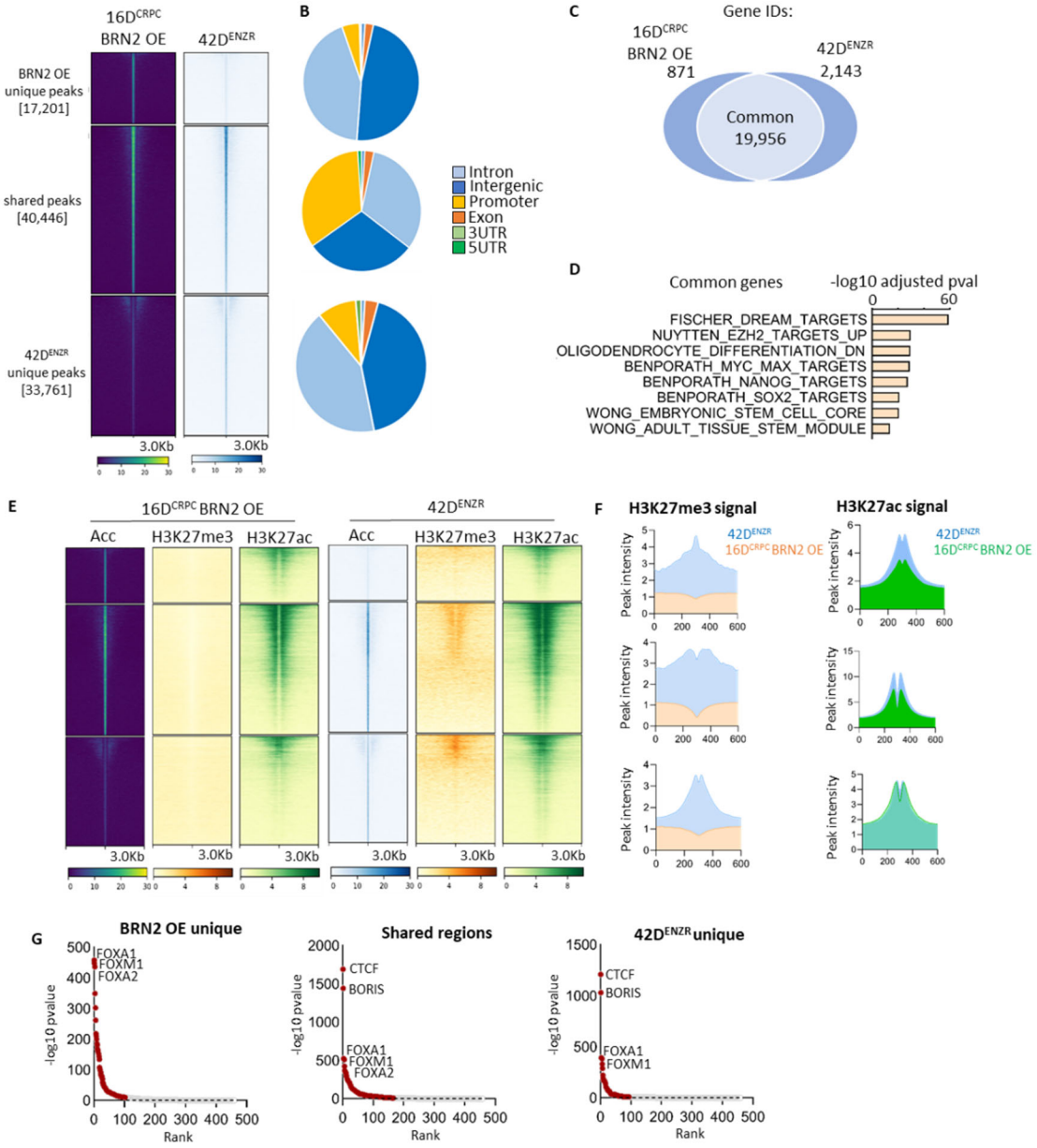

Figure 3: A) Heatmap shows lost regions in 16D^{CRPC} following overexpression of BRN2 for 72 hours in CRPC cell line and NEPC cell lines 42D^{ENZR}. **B)** Chromatin accessible annotations to promoter or non-promoter (enhancer) in regions lost after BRN2 overexpression (top), shared accessible regions between 16D^{CRPC} BRN2 overexpression and 42D^{ENZR} (middle), and accessible unique regions of 42D^{ENZR} (bottom). **C)** Common genes between 16D^{CRPC} BRN2 overexpression and 42D^{ENZR} **D)** Gene set enrichment analysis on genes up-regulated in NEPC (42D^{ENZR}) compared to CRPC (16D^{CRPC}) (top) or down-regulated in NEPC (42D^{ENZR}) compared to CRPC (16D^{CRPC}). p-value<0.05. **E)** Heatmap shows accessibility (ATAC-seq) and histone H3K27me3 and H3K27ac ChIP-seq in 16D^{CRPC} following overexpression of BRN2 for 72 hours in CRPC cell line and NEPC cell lines 42D^{ENZR}. **F)** Histogram shows H3K27me3 (left) and H3K27ac (right) peak intensity in regions unique to BRN2 overexpression for 72 hours in 16D^{CRPC} (top), shared accessible regions (middle), and regions unique to NEPC cell lines 42D^{ENZR} (bottom). **G)** Motif analysis comparing regions unique to 16D^{CRPC} overexpressing BRN2 (left), shared accessible regions (middle), and regions unique to NEPC cell lines 42D^{ENZR} (right). Motifs are ranked based on negative log10 of p-value.

Subtask 3: Interrogate the global effect of BRN2 inhibition on the chromatin structure in t-NEPC.
Zoubeidi

As a member of the POU-domain family transcription factors, BRN2 contains the POUS and POUH DNA binding domains (DBD) held together by a small but flexible linker sequence[25], which provides an attractive pocket for a small molecule. Herein, we generated a small molecule with enhanced potency and promising pharmacokinetic properties named 18-94, creating a potent chemical biology tool to study BRN2 inhibition in NEPC. In order to evaluate the on-target effect of the BRN2 inhibitor (BRN2i), we compared the effect to BRN2 knockout (BRN2-/-) using an inducible CRISPR/Cas9 system (Fig. 4A) to effects of BRN2i in both $42D^{ENZR}$ and 22RV1 cells. With the knockout confirmed by western blot, quantitative RT-PCR results showed that change in NEPC marker expression was comparable in $42D^{ENZR}$ and 22RV1 cells treated with BRN2i to that of the BRN2-/- cells (Fig. 4B-C). Overall, treatment with B18-94 downregulated both protein and mRNA levels of BRN2 itself and several of the known NEPC drivers/targets, e.g., ASCL1[9, 11], SOX2[26], EZH2[27], PEG10[28] and the NEPC marker CHGA in all 3 models (Fig.4B-E). We next performed RNA-seq using $42D^{ENZR}$ cells treated with BRN2i or with BRN2-/- and plotted the fold-change (FC) versus control for both conditions. We observed a significant correlation between the directionality of relative gene expression changes (up- or down-regulation) upon inhibition of BRN2 by B18-94 or BRN2-/- (Fig. 4F). Out of 1984 genes with -1 > log2FC > 1, the expression 1654 (84%), genes were concordant between both conditions. Upregulated genes (Q1) were enriched for epithelia development and apoptosis pathways, while downregulated genes (Q3) were enriched for cell cycle and neurogenesis pathways (Fig. 4G). Taken together, these data reveal a consistent reduction in cell proliferation as well as a switch from a neuronal to an epithelial phenotype upon either method of BRN2 inhibition. This high concordance led to a large overlap in biological clusters across gene sets. For example, there was a consistent downregulation of cell cycle/proliferation pathways, cell plasticity pathways related to neuronal differentiation, cancer stem cell (CSC) phenotype as well as the up-regulation of apoptosis and stress response pathways (Fig. 4H and I). Notably, RNA-seq further demonstrated the comparable downregulation of NEPC drivers/targets (e.g. ASCL1, SOX2, EZH2) (Fig. 4J) and NEPC markers (NCMA1, CHGA, CEACAM5/6) (Fig. 4J and K) by both BRN2i treatment and BRN2 knockout (Fig. 4J) mirroring the transcriptional changes induced by chemically distinct parental compounds (Fig. 4L). As expected for cells treated with a small molecule inhibitor, discordant genes (Q4) upregulated by BRN2i and not in BRN2-/- cells belong to small molecule metabolism pathways (Fig. 4M). Overall, these data clearly demonstrate that inhibition of BRN2 by BRN2i or genetic knockout affect the same biological pathways involved in cell plasticity and proliferation.

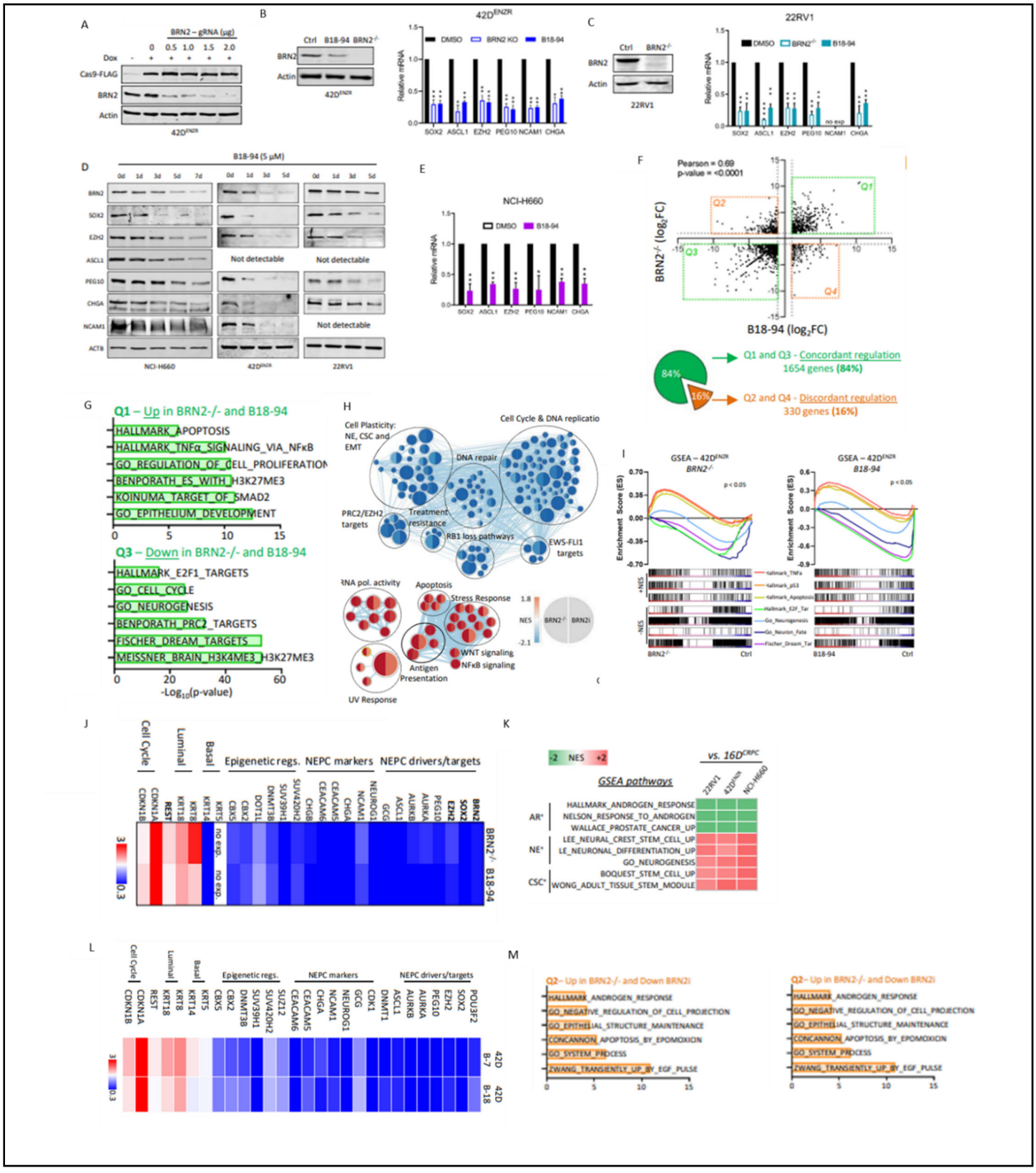
A
BRN2 – gRNA (μg)
0 0.5 1.0 1.5 2.0
Dox
Cas9-FLAG
BRN2
Actin
42D^ENZR
B
Ctrl B18-94 BRN2-/-
BRN2
Actin
42D^ENZR
42D^ENZR
DMSO BRN2 KO B18-94
Relative mRNA
SOX2 ASCL1 EZH2 PEG10 NCAM1 CHGA
C
Ctrl BRN2-/-
BRN2
Actin
22RV1
22RV1
DMSO BRN2-/- B18-94
Relative mRNA
no exp.
SOX2 ASCL1 EZH2 PEG10 NCAM1 CHGA
D
B18-94 (5 μM)
0d 1d 3d 5d 7d
BRN2
SOX2
EZH2
ASCL1
PEG10
CHGA
NCAM1
ACTB
Not detectable
NCI-H660
42D^ENZR
22RV1
E
NCI-H660
DMSO B18-94
Relative mRNA
SOX2 ASCL1 EZH2 PEG10 NCAM1 CHGA
F
Pearson = 0.69
p-value = <0.0001
Q1
Q2
Q3
Q4
BRN2-/- (log2FC)
B18-94 (log2FC)
84%
16%
Q1 and Q3 - Concordant regulation
1654 genes (84%)
Q2 and Q4 - Discordant regulation
330 genes (16%)
G
Q1 – Up in BRN2-/- and B18-94
HALLMARK_APOPTOSIS
HALLMARK_TNFα_SIGNALING_VIA_NFκB
GO_REGULATION_OF_CELL_PROLIFERATION
BENPORATH_ES_WITH_H3K27ME3
KOINUMA_TARGET_OF_SMAD2
GO_EPITHELIUM_DEVELOPMENT
Q3 – Down in BRN2-/- and B18-94
HALLMARK_E2F1_TARGETS
GO_CELL_CYCLE
GO_NEUROGENESIS
BENPORATH_PRC2_TARGETS
FISCHER_DREAM_TARGETS
MEISSNER_BRAIN_H3K4ME3_H3K27ME3
-Log10(p-value)
H
Cell Plasticity: NE, CSC and EMT
Cell Cycle & DNA replicatio
DNA repair
PRC2/EZH2 targets
Treatment resistance
RB1 loss pathways
EWS-FLI1 targets
RNA pol. activity
Apoptosis
Stress Response
NES
BRN2-/-
BRN2i
WNT signaling
NFκB signaling
Antigen Presentation
UV Response
I
GSEA – 42D^ENZR BRN2-/-
GSEA – 42D^ENZR B18-94
Enrichment Score (ES)
p < 0.05
+NES
-NES
Hallmark_TNFa
Hallmark_p53
Hallmark_Apoptosis
Hallmark_E2F_Tar
Go_Neurogenesis
Go_Neuron_Fate
Fischer_Dream_Tar
BRN2-/-
Ctrl
B18-94
Ctrl
J
Cell Cycle
Luminal
Basal
Epigenetic regs.
NEPC markers
NEPC drivers/targets
CDKN1B CDKN1A REST KRT18 KRT8 KRT14 KRT5 CBX5 CBX2 DOT1L DNMT3B SUV39H1 SUV420H2 CHGB CEACAM5 CEACAM6 CHGA NCAM1 NEUROG1 GCG ASCL1 AURKB AURKA PEG10 EZH2 SOX2 BRN2
no exp.
BRN2-/- B18-94
K
-2 NES +2
vs. 16D^CRPC
GSEA pathways
22RV1
42D^ENZR
NCI-H660
AR*
NE*
CSC*
HALLMARK_ANDROGEN_RESPONSE
NELSON_RESPONSE_TO_ANDROGEN
WALLACE_PROSTATE_CANCER_UP
LEE_NEURAL_CREST_STEM_CELL_UP
LE_NEURONAL_DIFFERENTIATION_UP
GO_NEUROGENESIS
BOQUEST_STEM_CELL_UP
WONG_ADULT_TISSUE_STEM_MODULE
L
Cell Cycle
Luminal
Basal
Epigenetic regs.
NEPC markers
NEPC drivers/targets
CDKN1B CDKN1A REST KRT18 KRT8 KRT14 KRT5 CBX5 CBX2 DNMT3B SUV39H1 SUZ12 SUV420H2 CEACAM6 CEACAM5 CHGA NCAM1 NEUROG1 GCG CDK1 DNMT1 ASCL1 AURKB AURKA PEG10 EZH2 SOX2 POU3F2
42D B-7
42D B-18
M
Q2– Up in BRN2-/- and Down BRN2i
HALLMARK_ANDROGEN_RESPONSE
GO_NEGATIVE_REGULATION_OF_CELL_PROJECTION
GO_EPITHELIAL_STRUCTURE_MAINTENANCE
CONCANNON_APOPTOSIS_BY_EPOMOXICIN
GO_SYSTEM_PROCESS
ZWANG_TRANSIENTLY_UP_BY_EGF_PULSE
Q2– Up in BRN2-/- and Down BRN2i
HALLMARK_ANDROGEN_RESPONSE
GO_NEGATIVE_REGULATION_OF_CELL_PROJECTION
GO_EPITHELIAL_STRUCTURE_MAINTENANCE
CONCANNON_APOPTOSIS_BY_EPOMOXICIN
GO_SYSTEM_PROCESS
ZWANG_TRANSIENTLY_UP_BY_EGF_PULSE

Figure 4: A) 42D^{ENZR} cells stable expressing rtA-eSpCas9-FLAG are treated with Doxycycline and with increased concentration of gRNA targeting Exon 1 of BRN2. **B)** Left: WB for BRN2 and Actin in 42D^{ENZR} cells treated with 5μM B18-94 or 2μg of gBRN2. Right: qRT-PCR comparing relative expression of BRN2 target genes upon treatment with B18-94 or BRN2 knockout via Cas9/gRNA. The results were reported as mean ± SD **C)** Left: WB validating BRN2 knockout in 22RV1 cells. Right: qRT-PCR comparing relative expression of BRN2 target genes upon treatment with B18-94 or BRN2 knockout via Cas9/gRNA. The results were reported as mean ± SD. **D)** Western blot for indicated genes in time-course of NCI-H660, 42D^{ENZR} and 22RV1 cells treated with 5μM of B18-94. **E)** qRT-PCR comparing relative expression of BRN2 target genes upon treatment with B18-94 in NCI-H660. **F)** RNA-seq comparing log2 (Fold Change vs. Control) between BRN2-/- and B18-94 treated 42D^{ENZR} cells. **G)** Pathways enriched in each quadrant with concordant and discordant regulation of genes between BRN2-/- and B18- 94. **H)** Biological clustering of GSEA up and downregulated in 42D^{ENZR} cells upon BRN2 inhibition via CRISPR/Cas9 or B18-94. **I)** Individual GSEA pathways for Apoptosis, Neuronal and Cell Cycle pathways upon inhibition of BRN2 by B18-94 or Cas9 mediated knockout. **J)** Change in expression of specific genes in 42D^{ENZR} cells with Cas9 mediated knockout of BRN2 compared to treatment with B18-94 for 48 hours. **K)** Heatmap of GSEA NES values comparing 22RV1, 42D^{ENZR} and NCI-H660 to 16D^{CRPC} cells. **L)** Change in expression of specific genes in 42D^{ENZR} cells with parental inhibitors B7 and B18 for 48 hours**. M)** Pathways enriched in Q2 and Q4 containing discordantly regulated genes between BRN2-/- and B18-94. * denotes p<0.05, ** denotes p<0.01, *** denotes p<0.001.

To interrogate this hypothesis, we analysed BRN2 binding to the chromatin using fractionation and ChIP-seq. We found that BRN2 inhibition using 18-94 drastically reduces the BRN2 bound to chromatin in a dose-dependent manner within 16 hours of treatment, without altering BRN2 nuclear localization. Importantly, overall transcription remained unaffected as RNA polymerase II (POL2RA) binding to the chromatin was unchanged (Fig. 5A). ChIP-seq analysis at the same time-point also confirmed that that BRN2i 18-94 significantly reduced BRN2 binding to chromatin (Fig. 5B). Moreover, upon analysis of the control (DMSO) ChIP-seq data, we can report for the first time, the BRN2 cistrome in both 42D^{ENZR} and NCI-H660 cells. We observed a strong consistency in biological pathways enriched in the genes with BRN2 binding sites, including neurogenesis and nervous system development (Fig. 5C and D). Within these pathways, specific loci of ASCL1 and SOX2, genes strongly correlated with BRN2 expression in multiple PCa datasets (Fig. 5E), and demonstrated a large reduction in BRN2 binding in the promoter region of both genes upon BRN2i B18- 94 treatment (Fig. 6F). This pattern was y observed in the NEPC marker PEG10 and BRN2 itself, further supporting the hypothesis for BRN2 auto-regulation[21, 29] (Fig. 5G). Importantly, the lack of BRN2 binding also significantly reduced the expression of ASCL1, SOX2 and BRN2 itself in both models by qRT-PCR prior to any observed reduction in BRN2 protein levels (Fig. 5H), suggesting that the transcriptional downregulation is due to inhibition of BRN2-chromatin interactions and not via translational and post-translational BRN2 protein modifications. These results were further confirmed by an unbiased approach of RNA-seq in both 42D^{ENZR} and NCI-H660 cells, as PEG10, ASCL1 and SOX2 were downregulated while enzymes implicated in small molecule metabolism like CYP1A223 and AKR1C224 were upregulated (Fig.5I). Similar to the data observed for 42D^{ENZR} cells, NCI-H660 cells also exhibited significant downregulation of NEPC drivers/targets/markers that are important for tNEPC progression (Fig. 5J). Biological similarity clustering of gene-set revealed consistent downregulation of cell proliferation, cell plasticity and DNA-repair pathways (a recently reported role of BRN2 in melanoma cells[30]), and upregulation of apoptosis (Fig. 5J and K). Cross-analysis of ChIP-seq and RNA-seq data revealed that the pathways enriched in the BRN2 cistrome like neurogenesis, nervous system development and EZH2/PRC2 targets, were all downregulated upon treatment with 18-94 in both 42D^{ENZR} and NCI-H660 cells (Fig. 5L). In concordance with loss of PRC2 activity, the consistently activated pathway included genes upregulated by siEZH2 treatment in PCa cells[31]. Altogether, these data indicate that BRN2i 18-94 halts BRN2 recruitment to chromatin and subsequently inhibits BRN2 transcriptional program that support the maintenance of NEPC and cell survival.

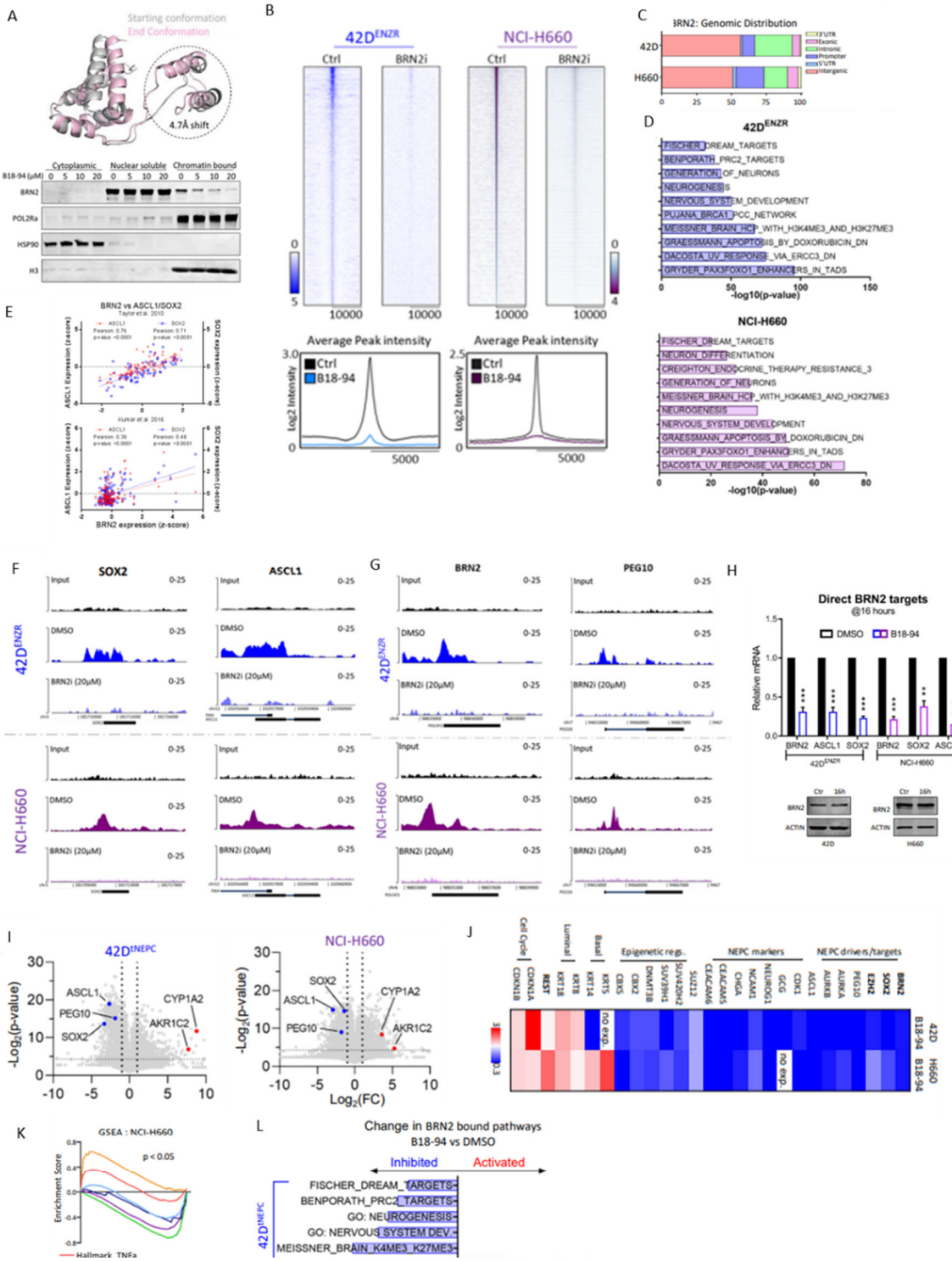

Figure 5. A) Predicted model on the effect of 18-94 binding to the DBD of BRN2. 42D^{ENZR} cells treated with BRN2i (18-94) 20μM for indicated time points and subject to sub-cellular fractionation**. B-D)** NCI-H660 and 42D^{ENZR} cells treated with BRN2i (18-94) 20μM. **B)** Heatmap for BRN2 binding -10000 to +10000 base pairs relative to transcription start sites. **C)** Annotated tracks from BRN2 ChIP-seq for ASCL1 and SOX2 loci in NCI-H660 and 42D^{ENZR} cells. **D-E)** RNA-seq analysis on NCI-H660 and 42D^{ENZR} cells treated with BRN2i (18-94). **D)** Volcano plot showing up-regulated and down-regulated genes. **E)** Biological clustering of upregulated and downregulated pathways upon BRN2 inhibition. **F)** Effect on BRN2 bound pathways in 42D^{ENZR} and NCI-H660 cells observed in **(B)** upon treatment with BRN2i 18-94 for 48 hours

To interrogate the global effect of BRN2 inhibition on the chromatin structure, we treated 42D^{ENZR} with our lead inhibitor 18-94 for 72 hours and performed ATAC-seq to measure global chromatin accessibility. We observed a significant number of regions gaining accessibility following BRN2 inhibition (86,642 BRN2i unique accessible regions), while only 7,656 regions were lost (CTL unique accessible regions) (Fig. 6A). Complementing our results that overexpression of BRN2 in 16D^{CRPC} decreases accessibility, we observed significant opening of the chromatin in NEPC treated with BRN2i. Notably, even within regions that were shared between BRN2i and control condition (66,289 BRN2i and CTL shared accessible regions) we observed an increase in ATAC-seq signal (Fig. 6B). Majority of altered regions were annotated to enhancer regions. However, there were more promoters associated with shared regions compared to regions gained accessibility following BRN2 inhibition (Fig. 6C). Investigating this further, we performed gene set enrichment analysis and identified both regions to be associated with pathways involve in regulating cell proliferation, differentiation and stemness (Fig. 6D). To better characterize the observed BRN2 dependent altered chromatin and the transcriptomic output of this remodelling, we integrated our RNA-seq data in NEPC following treatment with our lead compound and segregated genes into up- or down-regulated (Fig. 6E), followed by pathway enrichment analysis (Fig. 6F). Both BRN2 dependent and independent accessible regions were heavily associated with proliferation and cell cycle as well as plasticity pathways (Fig. 6F), supporting the hypothesis that targeting BRN2 in NEPC, using our small molecule, may decreases cell proliferation *in vitro* and tumor growth *in vivo* and abrogate the NE phenotype.

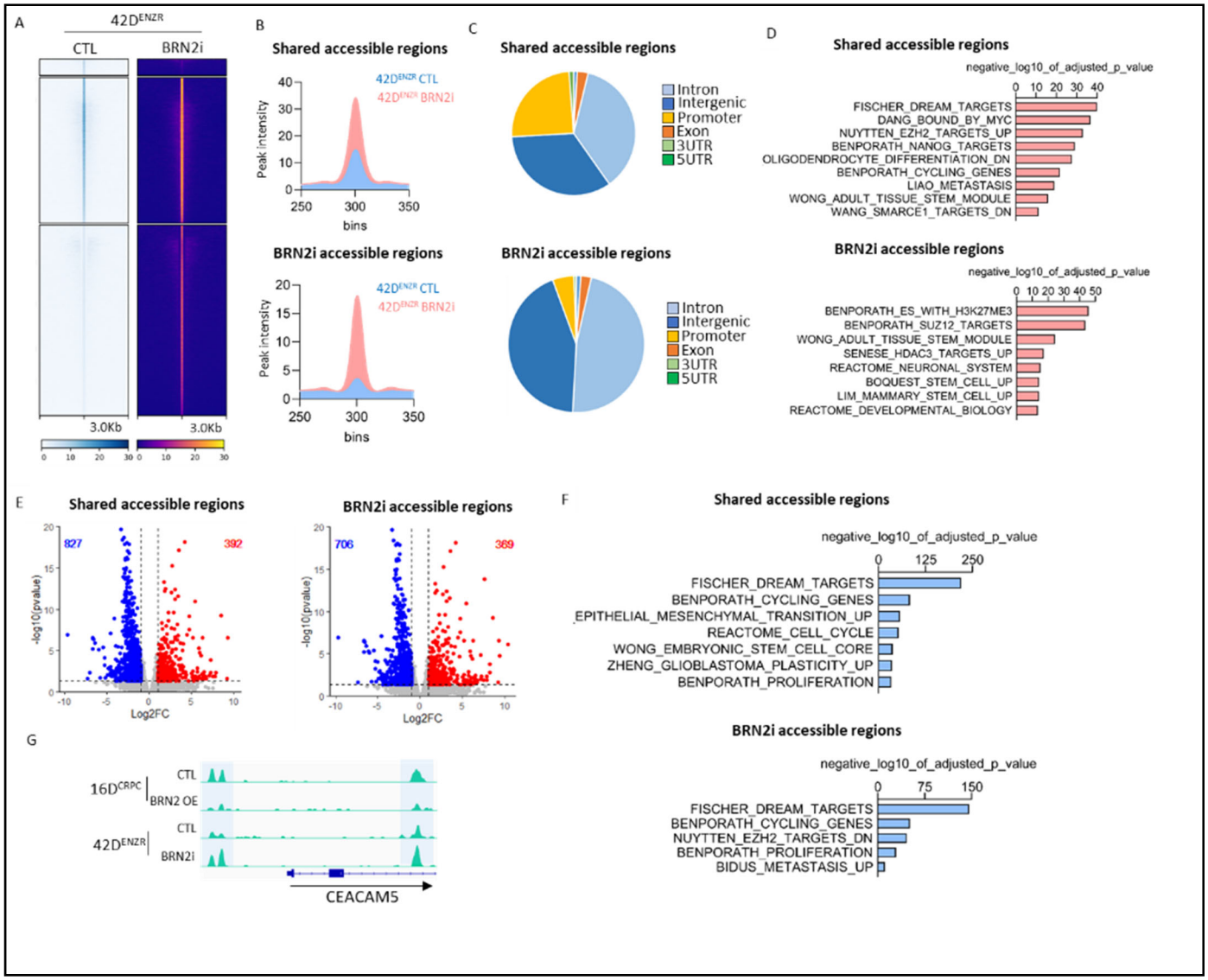

Figure 6. A) Heatmap for BRN2 ChIP-seq in 42D^{ENZR} CTL and following BRN2 inhibition using 18-94 compound for 72 hours. **B)** Histogram shows shared accessible regions (top) and regions unique to 42D^{ENZR} BRN2 inhibition (bottom) signal peak intensity. **C)** Chromatin accessible annotations to promoter or non-promoter (enhancer) in regions unique to 42D^{ENZR} BRN2 inhibition (top), and shared accessible regions between 42D^{ENZR} CTL and following BRN2 inhibition using 18-94 compound for 72 hours (bottom). **D)** Gene set enrichment analysis on genes accessible in 42D^{ENZR} CTL and following BRN2 inhibition using 18-94 compound for 72 hours (top) and genes unique to 42D^{ENZR} BRN2 inhibition (bottom). p-value<0.05. **E)** Volcano plot shows expression of accessible common genes (left) and genes unique to 42D^{ENZR} BRN2 inhibition (right) in 42D^{ENZR} following BRN2 inhibition using 18-94 compound for 72 hours compared to control. Each dot represents one gene. **F)** Gene set enrichment analysis on genes accessible and downregulated in 42D^{ENZR} following BRN2 inhibition using 18-94 compound for 72 hours (top) and genes unique to 42D^{ENZR} BRN2 inhibition (bottom) compared to control. p-value<0.05. **G)** Tracks showing chromatin accessibility surrounding CEACAM5 promoter in 42D^{ENZR} CTL and following BRN2 inhibition using 18-94 compound for 72 hours as well as in 16D^{CRPC} CTL and following BRN2 overexpression for 72 hours.

Subtask 4: Identify the epigenetic, transcriptional and co-activator network downstream of BRN2 that confers the reprogramming from Adenocarcinoma to NEPC.
Zoubeidi

Next, to identify BRN2 epigenetic and transcriptional co-activators, we performed large-scale integrated genome analysis (GIGGLE)[32] to pinpoint loci highly correlated with BRN2. Specifically, we aimed to understand co-factors which assist BRN2 in regulating chromatin accessibility and deposition of histone marks. Therefore, we overlapped the genomic coordinates of BRN2-dependent inaccessible regions with those identified in publicly available ChIP-seq datasets (n= 13,976) Cistrome DB. We segregated our hits into transcription factors and epigenetic factors (Fig. 7A). We observed a correlation between BRN2-dependent inaccessible regions and CTCF. On the other hand, among the epigenetic factors we observed a correlation between members of SWI/SNF complex (ARID1A and SMARCC1), an ATPase-dependent chromatin remodeller and EP300, histone acetyltransferase. These observation observations are in alignment with BRN2 pioneering activity. Our data suggests that BRN2 may cooperate with CTCF and SWI/SNF complex to reorganize the chromatin structure, while in concert with EP300 deposit histone acetylation. This observation was in alignment with our data showing that BRN2 overexpression remodels the chromatin structure and increases H3K27ac, similar to NEPC.

SWI/SNF complex is a highly conserved multi-protein ATP-dependent chromatin remodeling complex[33, 34] implicated in the control of transcriptional programs mediating cell differentiation and lineage specification[35, 36]. It contains one of the two catalytic subunits, SMARCA2 or SMARCA4, that possess DNA-stimulated ATPase activity for chromatin remodeling[37-40]. Distinct assemblies of the SWI/SNF complex have been identified, including the neural progenitors and post-mitotic neurons[36]. During the differentiation of neural progenitor cells to neurons, the SWI/SNF complex undergoes a dynamic compositional switch from neural progenitors (containing specific subunits: ACTL6A, PHF10, and SS18) to post-mitotic neurons (containing specific subunits: ACTL6B, DPF1, and SS18L1)[41]. Alterations of SWI/SNF subunits occur in approximately 20% of cancer cases[42, 43], including PCa[44, 45], and can confer tumour-suppressive[42, 46-48] or tumour-promoting[49-51] functions. In PCa adenocarcinoma, SWI/SNF co-operates with AR to support the luminal phenotype by binding to and activating AR[52, 53] and cell proliferation[54, 55]. Targeting SWI/SNF by dual degradation of SMARCA2 and SMARCA4 reduces chromatin accessibility at the enhancers and decreases tumour growth in PCa adenocarcinoma[56]. Interestingly, the expression SMARCA4 is higher in NEPC compared to PCa adenocarcinoma [44]. However, SWI/SNF function in ARPI-induced NEPC is not yet explored. Our data suggest that BRN2 may function in collaboration with SWI/SNF to exert its pioneering activity, orchestrating chromatin remodeling and transcriptional rewiring to facilitate lineage plasticity and NEPC differentiation. To this end, we performed rapid immunoprecipitation mass spectrometry of endogenous proteins (RIME)[57] in NEPC cell lines 42D^{ENZR} and NCI-H660 using BRN2 as bait. Proteins with <2 peptide spectrum matches or zero unique peptides were filtered out. Proteins with at least 10-fold abundance in the samples compared to IgG, and identified in at least 2 out of 3 replicates were considered as interactors as previously described[58]. Specifically, we segregated proteins common between the two NEPC

cell lines (Fig. 7B). In further support of this hypothesis that BRN2 may cooperate with chromatin remodeler SWI/SNF in modulating the chromatin structure, our RIME experiment identified that BRN2 interacts with many components of the SWI/SNF complex (Fig. 7C). The interaction between BRN2 and ARID1A was validated by co-immunoprecipitation (Fig. 7D). Overall, we can hypothesize that as BRN2 expression increases upon treatment with anti-androgens due to AR suppression, it co-operates with powerful epigenetic elements such as the SWI/SNF complex and remodels the chromatin leading to increased expression of genes involved in cell plasticity.

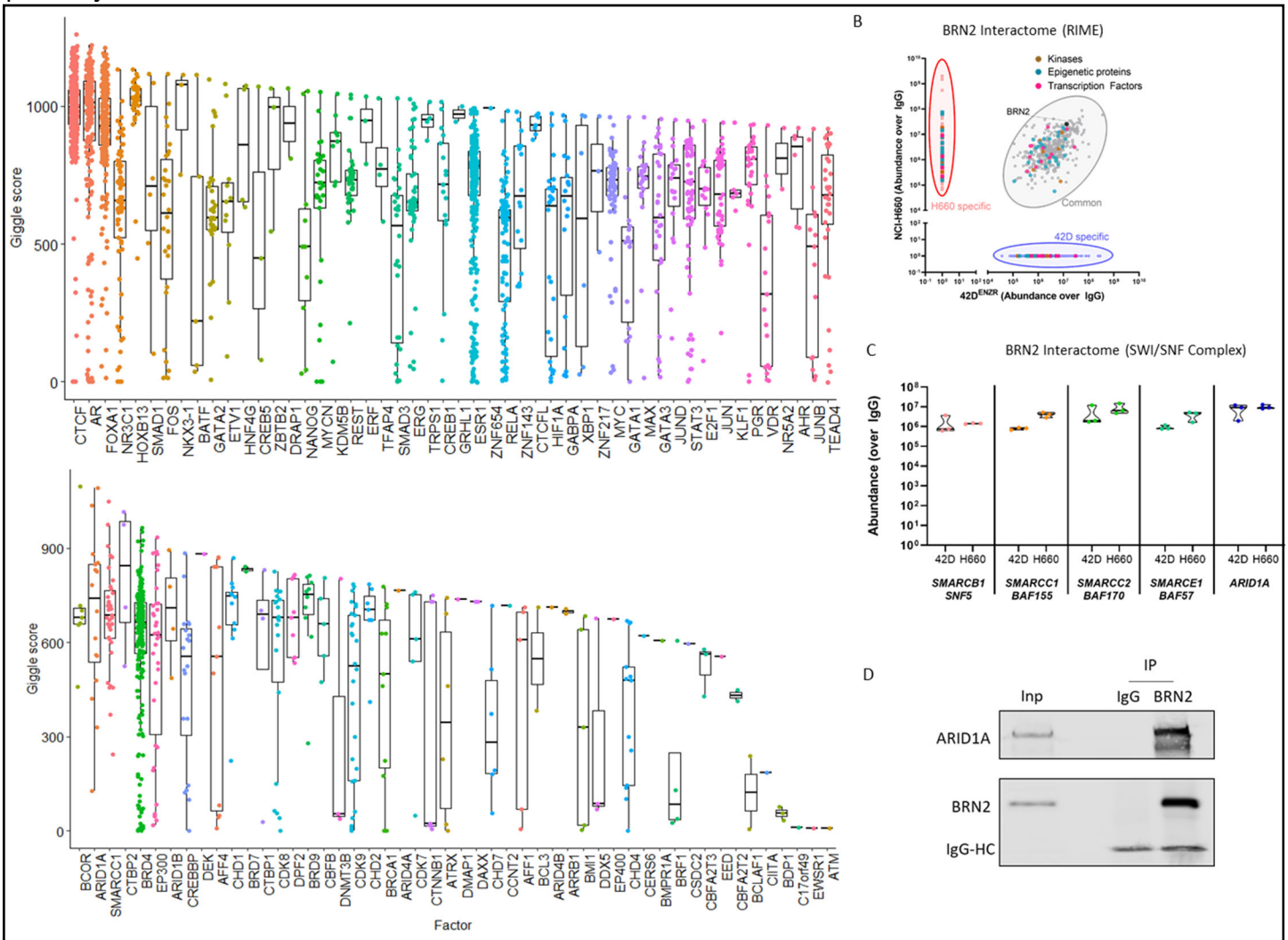

Figure 7: A) GIGGLE analysis using BRN2-dependent inaccessible regions lost in CRPC following BRN2 overexpression as query showing transcription factors (left) and epigenetic factors (right). **B)** RIME using BRN2 as bait in NEPC cell lines 42D^{ENZR} and NCI-H660 shows BRN2 interactome unique to each cell line and common between the two. **C)** Members of SWI/SNF complex identified in RIME experiment as abundance over IgG. **D)** Co-immunoprecipitation using BRN2 as bait and blotted for BRN2 and ARID1A (member of the SWI/SNF complex). IgG was used as a control.

To identify the transcriptional networks downstream of BRN2 that confers the reprogramming from Adenocarcinoma to NEPC, we performed in depth analysis of BRN2 ChIP-seq. We started by defining a consensus set of BRN2 DNA binding locations (peaks) using MACS2 (q<0.5) in 42D^{ENZR} cells replicates. Next, to define a robust, reproducible set of BRN2 peaks across multiple cell types, BRN2 peaks shared by at least 3 out of 4 of the following 4 cell lines were identified: 42D^{ENZR} (consensus peaks, as above), NCI-H660 (one BRN2

ChIP-seq performed by the Zoubeidi Lab), and the neural-like lung squamous cell carcinoma (LUSC) cell lines LK2 and NCI-H520 (one publicly available BRN2 ChIP-seq peak set each[16]).

To identify a set of putative BRN2 target genes corresponding to the reproducible set of BRN2 ChIP-seq peaks defined above, we annotated that set of BRN2 peaks using UROPA[59] with the following strategy: peaks in the promoter region (-1 kb to +100 bp) of a known protein-coding gene were annotated with that gene only; otherwise, peaks were annotated with any gene that overlapped the peak and with any gene whose 5' end was within 25 kb of the peak. To determine which putative BRN2 target genes are likely to be positively or negatively regulated by BRN2, we computed expression correlations of all genes with POU3F2 in publicly available RNA-seq data from 4 PCa patient cohorts[8, 60, 61]. Specifically, for all genes with available expression data, their Spearman and Pearson correlations with POU3F2 expression (after log2 transformation) were computed separately for each dataset and the resulting left- and right-sided p values were combined across datasets using Liptak's weighted "inverse normal" method (in the metaRNAseq R package). The combined p values were then adjusted for multiple hypothesis testing using the Benjamini-Hochberg (BH) method. Genes were considered to have expression significantly positively correlated with POU3F2 if either (1) their Spearman correlation was ≥0.3 with right-sided p value ≤0.05/2 and their Pearson correlation was ≥0.1 or (2) their Pearson correlation was ≥0.3 with right-sided p value ≤0.05/2 and their Spearman correlation was ≥0.1. Significantly negatively correlated genes were defined analogously (using left-sided p values and negative correlations). As a result, we defined a positive and a negative BRN2 signatures (scores) (Table 1 and 2) as the sets of putative BRN2 target genes positively and negatively correlated, respectively, with POU3F2 expression.

BRN2 positive score				
EXOSC10	ENO2	WRAP53	FRG1HP	MAP3K7
CDC20	TROAP	KPNA2	CDC25B	WDR27
RN7SKP285	KSR2	MYBL1	NANP	MCM4
SMG7-AS1	RFC5	NPTX1	TTLL9	
SPRTN	POLE	CHAF1A	PAXBP1	
DNAJC19P1	CEP128	NRTN	IFT80	
HELLS	BUB1B	ZNF317	SMC4	
UHRF2	ZWILCH	SCGB2B2	NCAPG	
CCDC77	SPATA33	ZNF850	ABCC10	
UPF3B	HASPIN	SPC25	EFHC1	

Table 1: BRN2 positive score

BRN2 netative score
MICOS10
DCAF6
C1orf116
NCOA4
CAB39L
RPS2
NAA60
GCAT
MDH2

Table 2: BRN2 negative score

To validate our signature, we use the signature to compare enrichment in 16D^{CRPC} and NCI-H660. We observed enrichment of BRN2 positive score in NCI-H660, while BRN2 negative score was enriched in 16D^{CRPC} (Fig. 8A). Further validating our generated BRN2 signature, we observed enrichment of BRN2 positive score in both 42DENZR and NCI-H660 DMSO compared to treatment with BRN2i (Fig. 8B).

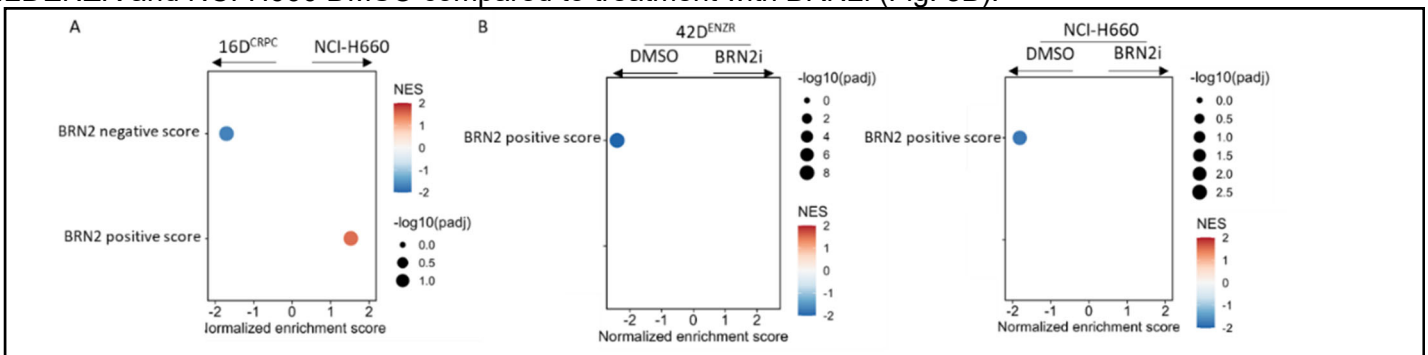

Figure 8: BRN2 positive and negative score in **A)** 16D^{CRPC} and NCI-H660 and **B)** 42D^{ENZR}, and **C)** NCI-H660 treated with BRN2i 18-94 for 72 hours. Data is presented as normalized enrichment score (NES).

Milestone #1: Develop manuscript delineating BRN2's role in epigenetic remodeling resulting in transformation from Adenocarcinoma to NEPC.

This milestone has been successfully accomplished through the comprehensive development of a manuscript that elucidates the central involvement of the BRN2 transcription factor in epigenetic remodelling, resulting in the transformation of adenocarcinoma to NEPC. We are preparing a manuscript titled: "BRN2-Mediated Chromatin Remodeling in Neuroendocrine Prostate Cancer". Our data generated within this aim advanced our understanding of NEPC progression and the role of BRN2 in influencing NEPC trans-differentiation.

SPECIFIC AIM 2: EVALUATE PHARMACOLOGICAL AGENTS TARGETING BRN2 EXPRESSING CRPC PDX MODELS ALONE OR IN COMBINATION WITH CARBOPLATIN TO CONFIRM ANTI-TUMOR EFFECTS AND SUPPORT FURTHER CLINICAL EVALUATION.

Subtask 1: Evaluate the BRN2 inhibitor alone and in combination with carboplatin in 4 PDX lines. Perform animal studies, measure tumor volumes, body weight, and survival and isolate frozen and paraffin embedded tissue in four BRN2+.
Corey, Morrissey, Zoubeidi

The pharmacokinetic and toxicity profile of our lead BRN2i 18-94 were characterized using the Nu/Nu murine model. We tested BRN2i B18-94 bioavailability with both intra-peritoneal (IP) and per os (PO) routes of administration. Interestingly, both methods converged in their serum concentrations at approximately 8 hours (Fig. 9A). With a calculated half-life of approximately 4.1 hours (Fig. 9B), we proceeded with PO dosing and conducted a multi-dose toxicity study. We discovered that BRN2i 18-94 is well tolerated even at 200 mg/kg without any weight loss or neurotoxicity symptoms (lethargy and repetitive actions) for up to 2 weeks of treatment (Fig. 9B). Taking the 50 and 200 mg/kg doses, we performed an *in vivo* dose response experiment with NCI-H660 xenografts and found no significant advantage from the higher dose (Fig. 9C). Subsequent studies with larger number of animals per arm clearly demonstrated that 50 mg/kg dose of BRN2i 18-94 significantly reduced tumor volume of $42D^{ENZR}$ and NCI-H660 xenograft (Fig. 9D and E). Additionally, BRN2i 18-94-treated tumors had significantly reduced transcript levels of BRN2, SOX2, ASCL1 and PEG10 (Fig. 9D and E). Lastly, we compared the efficacy of BRN2i 18-94 to standard of care platinum-based chemotherapy using the NCI-H660 xenografts. The 50 mg/kg dose of BRN2i 18-94 demonstrated comparable anti-tumor activity to 20 mg/kg dose of carboplatin, however in contrast to carboplatin without the toxicity induced weight loss (Fig. 9F).

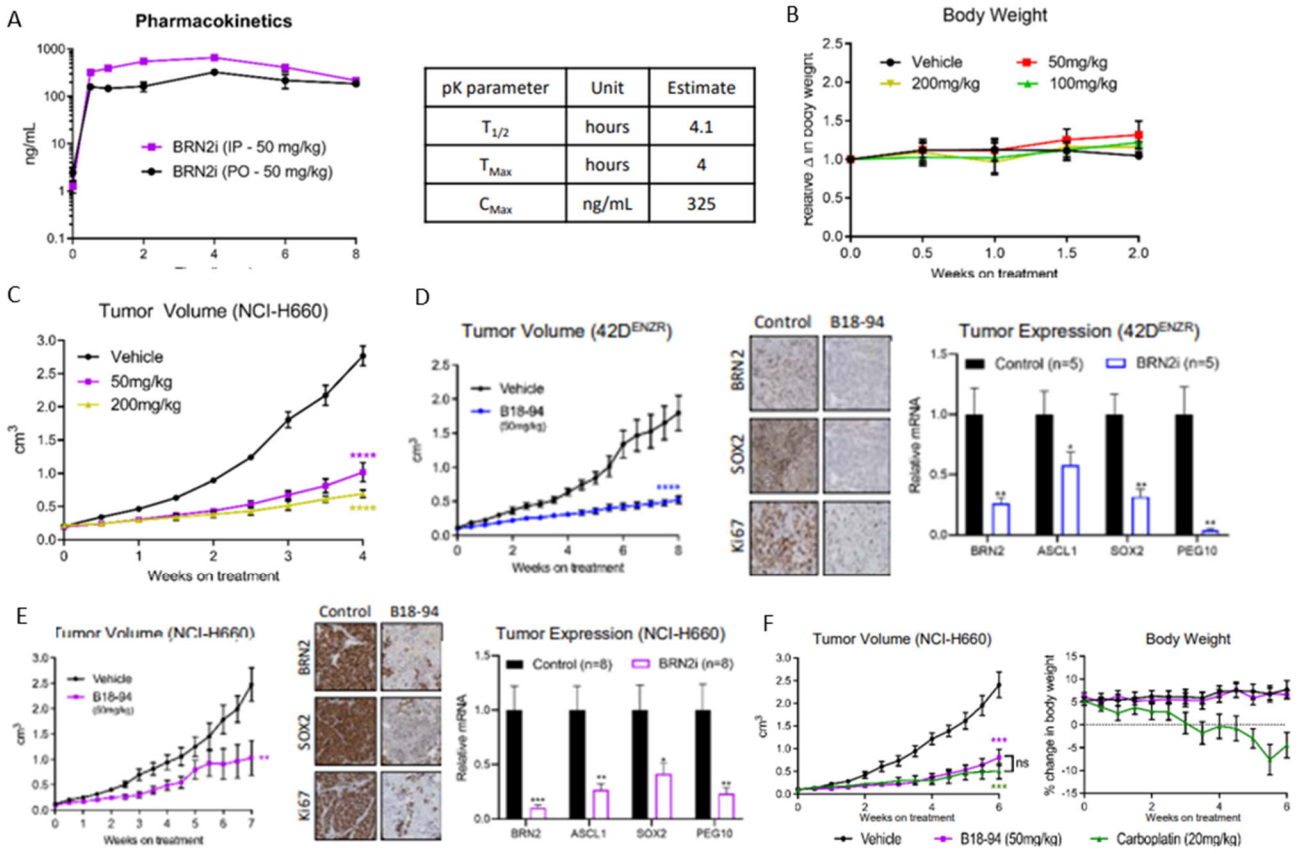

pK parameter	Unit	Estimate
$T_{1/2}$	hours	4.1
T_{Max}	hours	4
C_{Max}	ng/mL	325

Figure 9: Xenograft of 42D^{ENZR} and NCI-H660 injected into Nu/Nu mice. Mice were treated with indicated doses of 18-94 when tumor volume reached 100mm3. **A)** Tumor volume of 42D^{ENZR} xenografts treated with control (n=7) and 50mg/kg of 18-94 (n=10), IHC staining and qRT-PCR for indicated target genes. The results were reported as mean ± SEM; * denotes p<0.05, ** denotes p<0.01, *** denotes p<0.001, **** denotes p<0.0001. **B)** Tumor volume of NCI-H660 xenografts treated with control (n=8) and 50mg/kg of B18-94 (n=9), IHC staining and qPCR for indicated target genes. The results were reported as mean ± SEM; * denotes p<0.05, ** denotes p<0.01, *** denotes p<0.001. **C)** Tumor volume and change in body weight of NCI-H660 xenografts treated with vehicle (n=5), carboplatin (n=5) and 18-94 (n=6). The results were reported as mean ± SEM; *** denotes p<0.001

To extend the preclinical testing, we set up to evaluate the efficacy of BRN2i 18-94 in NEPC PDX models. First, we interrogated BRN2 (POU3F2) expression in the NEPC PDX models to identify appropriate models for these studies. We identified BRN2 (POU3F2)-positive and negative NEPC PDXs by RNA-Seq (Fig. 10A) and immunohistochemistry (Fig. 10B).

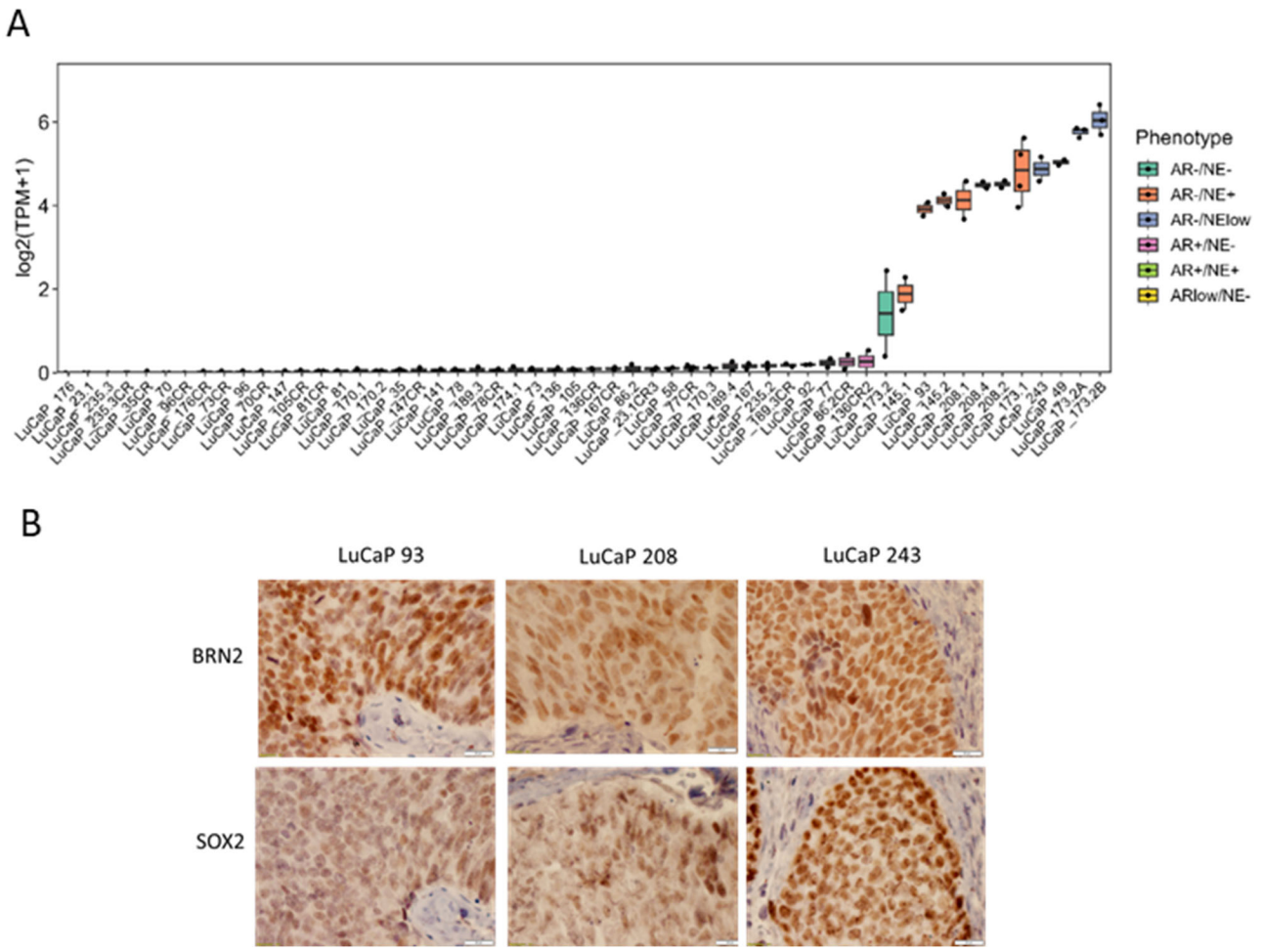

Figure 10: A) POU3F2 expression in LuCaP PDX models. **B)** IHC showing BRN2 and SOX2 expression in the NEPC LuCaP PDX models.

The first two PDX lines studied were LuCaP 93 (high expresser) and LuCaP 145.2 (little to no expression. Unfortunately, in these two studies we observed toxicity of the BRN2i 18-94, and had to decrease the BRN2i dose. Ultimately, we did not observe any significant change in tumor volume in either LuCaP 93 or LuCaP 145.2 after treatment with the BRN2i 18-94 (Fig. 11).

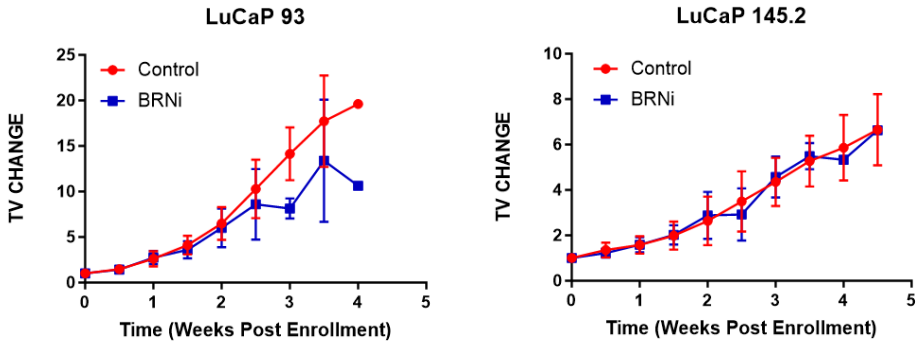

Figure 11: Tumor volume (TV) change in vehicle control and BRN2i treated LuCaP 93 and LuCaP 145.2 NEPC PDX models.

To interrogate potential factors involved in no efficacy of the BRN2i 18-94 in these two studies we set up to confirm BRN2 expression in both PDXs used and to evaluate whether BRN2 expression was altered after BRN2i 18-94 treatment. We assessed all tumors from both studies for BRN2 expression by RNA-seq and IHC. As expected LuCaP 93 was positive for BRN2, whereas LuCaP 145.2 was not. We also did not observe any significant difference in BRN2 expression in tumors from BRN2i 18-94-treated compared to untreated animals (LuCaP 93 p=0.18). We hypothesized that the low dose of the inhibitor used due to observed toxicity might have been the reason for the negative results. We considered that the toxicity could be related to the specific batch of the inhibitor used or mice strain. To address this issue, we prepared a new batch of the BRN2i 18-94 and tested its toxicity. For the PDX studies we used CB17 SCID mice, a different mouse strain from the cell line xenograft studies, and therefore we tested potential BRN2i toxicity in CB17 SCID mice, with increasing dose from 30 to 50 to 75 up to 100 mg/kg. In this experiment, all the doses were well tolerated in SCID mice. Thus, we proceeded and ran additional preclinical studies using five NEPC PDX models: LuCaP 49, 173.1, 208.4, 243, and 93. Unfortunately, even with the 100 mg/kg BRN2i 18-94 dose, our results showed that overall, the BRN2i 18-94 treatment did not affect growth of these PDX models (Fig. 12). As proposed, we also investigated whether combination of BRN2i 18-94 with carboplatin can provide improvement in efficacy of the BRN2i monotherapy. In these studies, we used LuCaP 93 and LuCaP 243. Treatment of LuCaP 93 with carboplatin inhibited tumor progression, and the combination treatment of BRN2i 18-94 and carboplatin exhibited similar effects to carboplatin monotherapy. Similar results were observed using LuCaP 243.

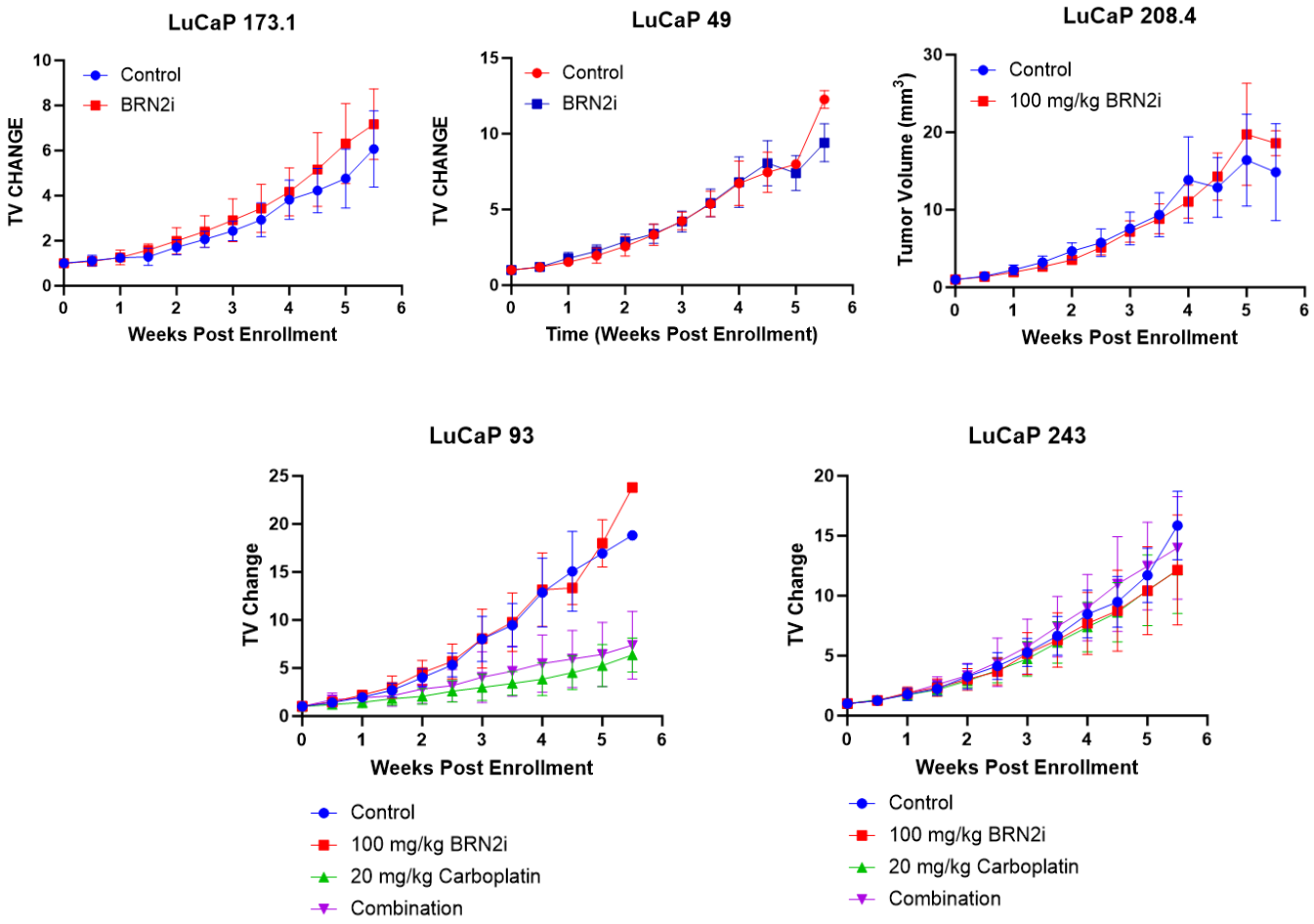

Figure 12: Tumor volume (TV) change in vehicle control and BRN2i treated LuCaP 173.1, LuCaP 49, LuCaP 208.4, and vehicle control, BRN2i, carboplatin, and carboplatin/BRN2i treated LuCaP 93 and LuCaP 243 NEPC PDX models.

Subtask 2: Evaluate the BRN2 inhibitor alone and in combination with Enzalutamide in 1-2 AR+ CRPC PDX lines. Perform animal studies, measure tumor volumes, body weight, and survival and isolate frozen and paraffin embedded tissue.
Corey, Morrissey

We have evaluated all of the AR-positive LuCaP PDX models available for POU3F2/BRN2 expression and did not detect any expression of POU3F2 mRNA or BRN2 protein and therefore we did not perform these experiments. Instead we increased number of PDX models in which we evaluated efficacy of BRN2i 18-94 as monotherapy (Fig 11 and 12).

Subtask 3: Assess molecular features of response and emergent resistance mechanism(s) from specimens obtained from the *in vivo* studies. RNA-seq, Western analysis, IHC.

Zoubeidi, Corey, Morrissey

RNA-seq was performed on end-of-study and on-study tumors for each of the animal studies. Differences in gene expression using gene set enrichment analysis for hallmark pathways are described for each of the BRN2i treated lines with an n=3 tumors / group (Fig. 13 through 14). No significant changes were consistently observed in the RNA-seq data from the end-of-study LuCaP PDX lines. However, significant consistent increases in

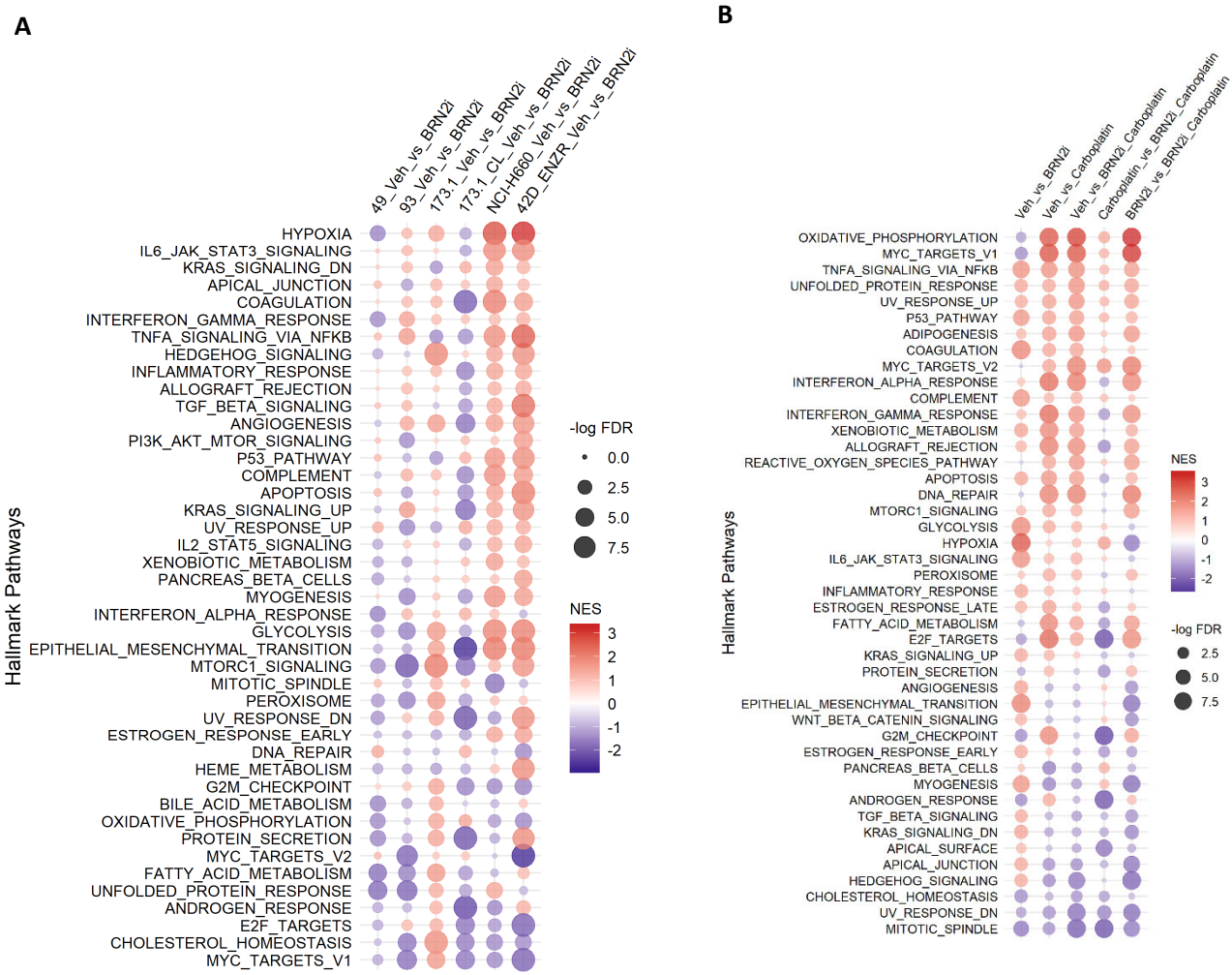

Figure 13: A) GSEA Pathways with FDR<0.05 in at least one comparison for each *in vivo* study in vehicle control and BRN2i treated LuCaP 49, LuCaP 93, LuCaP 173.1, NCIH660, and 42D cells. **B)** GSEA Pathways with FDR<0.05 in at least one comparison for each *in vivo* study in vehicle control versus BRN2i, versus carboplatin, versus BRN2i plus carboplatin, carboplatin versus BRN2i plus carboplatin and BRN2i versus BRN2i plus carboplatin treated NCIH660 xenografts.

HYPOXIA, IL6_JAK_STAT3_signaling, TNFASIGNALING_VIA_NFKB, and APOPTOSIS among other pathways were significantly changed in the NCIH660 and 42D lines (Fig. 13A). Mirroring the response of the changes in tumor volume in each of the lines. Changes in OXIDATIVE_PHOSPHORYLATION,

MYC_TARGETS_V1, and MYC_TARGETS_V2 pathways were altered with carboplatin treatment in NCIH660 xenografts. With a decrease in MITOTIC_SPINDLE in both BRN2i and carboplatin treated tumors, which was more pronounced in BRN2i plus carboplatin treated animals, consistent with an increased effect if dual BRN2i/carboplatin treatment of NCIH660 cells (Fig. 13B).

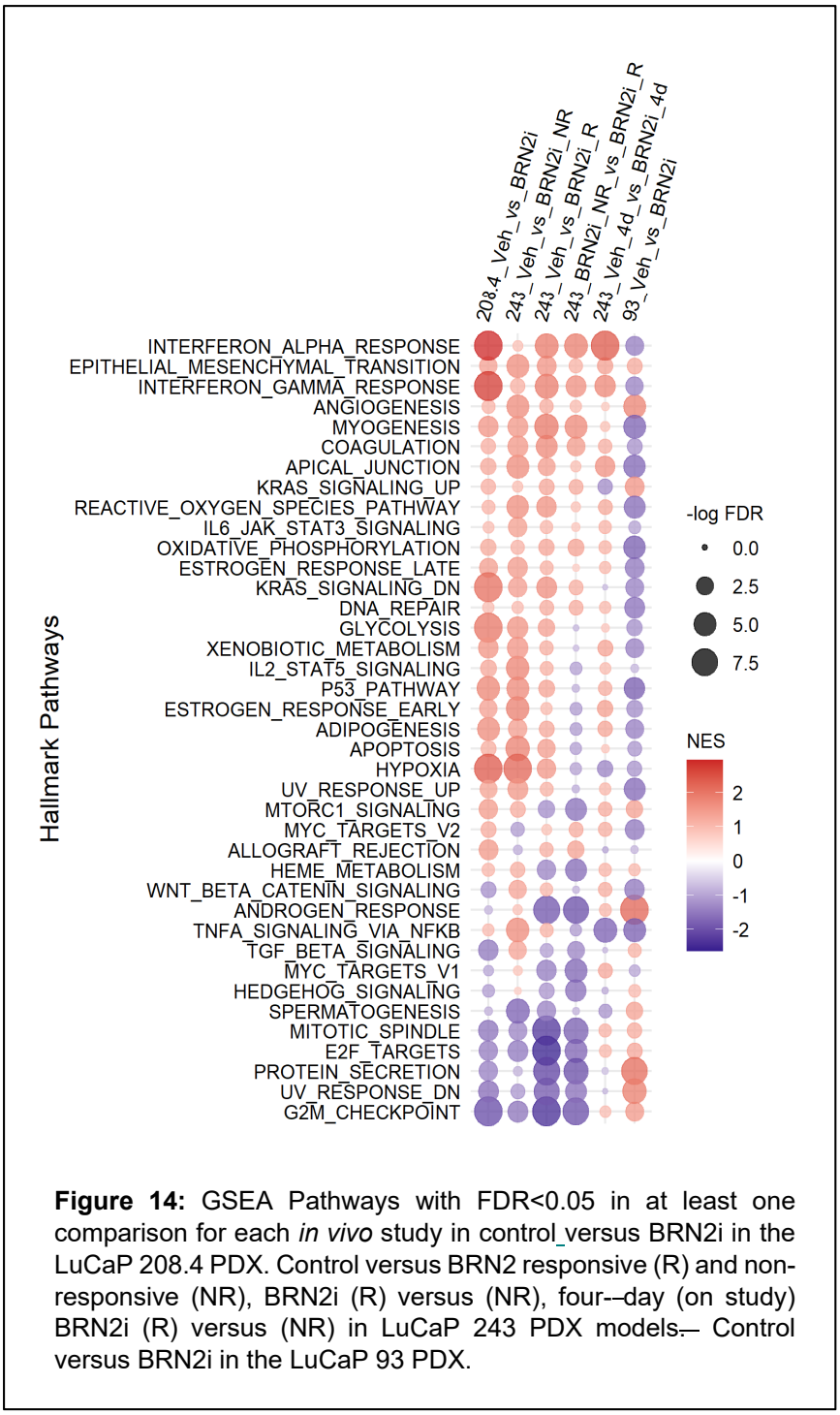

Figure 14: GSEA Pathways with FDR<0.05 in at least one comparison for each *in vivo* study in control versus BRN2i in the LuCaP 208.4 PDX. Control versus BRN2 responsive (R) and non-responsive (NR), BRN2i (R) versus (NR), four-day (on study) BRN2i (R) versus (NR) in LuCaP 243 PDX models. Control versus BRN2i in the LuCaP 93 PDX.

RNA-seq was performed for LuCaP 93, LuCaP 208.4, and LuCaP 243 NEPC PDX lines (Fig. 14). In one model, LuCaP 243, we observed variability of the responses of the individual tumors, and identified 3 animals in which the tumor progression was inhibited (Fig. 15A and B**)**. RNA was extracted from control, BRN2i not inhibited and BRN2i inhibited LuCaP 243 tumors (Fig. 15B) and RNA-Seq was used to evaluate the differences in these tumors that could be responsible for the BRN2 inhibition of the tumor progression or possible mechanisms of resistance in the non-responder groups. We performed principal component analysis and could not observed distinctive clustering between control, BRN2i not inhibited and BRN2i inhibited LuCaP 243 tumors (Fig. 15C). Next, we performed differential gene expression analysis using edgeR, DESeq2, limma, and NOISeq programs in R. The median *q* value (BH-adjusted *p* value) from the 4 methods was used to measure significance of differential expression. A minimum absolute $\log_2$ (fold change) of $\log_2(1.1)$ was built into the statistical testing for edgeR, DESeq2, and limma. For each of edgeR, DESeq2, and limma, a single generalized linear model that included all sample groups was fitted with the LuCaP identity, treatments, and response (encoded as "NA" when not known) all included as variables in the design matrix, and the desired contrasts were extracted from that model for different comparisons of interest. Comparison of BRN2i-treated-responders vs control LuCaP 243 PDXs yielded some differentially expressed genes. Performing gene set enrichment analysis, we observed a number of pathways to be affected by the inhibitor (Fig. 15D and E). Inflammation pathways were significantly increased in the responsive xenograft tumors and proliferation-associated pathways were significantly decreased upon treatment with BRN2i (Fig. 15D and E), which correlates with reduced proliferation rate of the responder group. Likewise, we compared BRN2i-treated-non-responders vs control LuCaP243 PDXs and observed several differentially regulated genes. We observed alteration of some of the similar pathways as

in the responder groups vs control group (Fig. 15F and G). However, what was uniquely different between responders and non-responders when compared to control untreated tumors, was downregulation of cell cycle and increase of xenobiotic metabolism (related to small molecule metabolism) in responders. To further delineate the molecular features of responders, we performed comparison of BRN2i-treated LuCaP 243 responders vs non-responders. This analysis did not reveal any significantly differentially expressed genes at the 5% FDR level. This suggests that the post-treatment tumor cells sampled from the responder group may be the resistant cells selected for by the BRN2i treatment and the cell actually responded to treatment might have not been captured.

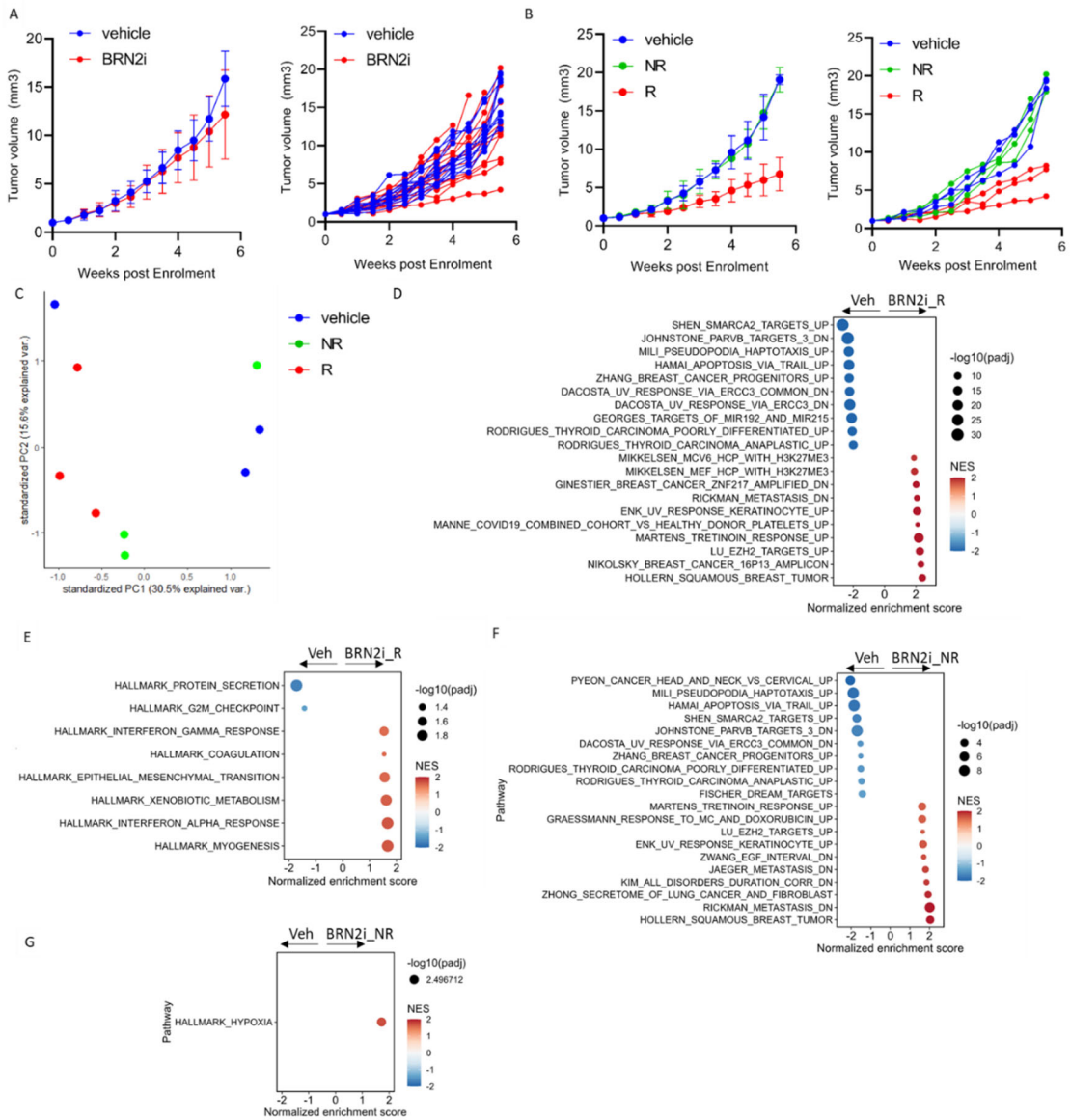

Figure 15: (A) LuCaP PDX 243 treated with vehicle or BRN2i 18-94 100 mg/kg TV. **(B)** LuCaP PDX 243 treated with vehicle or BRN2i 18-94 100 mg/kg shows a group of responders (R) and non-responders (NR). **(C and E)** Principle component analysis (PCA) shows separation of each sample. **(D)** Gene set enrichment analysis comparing BRN2i 18-94 responders to control. **(F and G)** Gene set enrichment analysis comparing BRN2i non-responders to control.

Subtask 4: Discuss the development of clinical trial concepts with institutional physicians based on positive preclinical results
Zoubeidi, Corey, Morrissey

Unfortunately, our *in vivo* PDX experiments did not yield the desired results. During these experiments, we encountered toxicity issues, which prompted us to reduce the administered dose of the treatment. However, despite this adjustment, we did not observe any discernible response in the experimental subjects. As a result, we are in the process to re-evaluate our approach, consider alternative strategies, and possibly explore modifications to the treatment regimen or compound itself in order to address the observed toxicity and lack of response. This setback, while disappointing, serves as a valuable learning experience as we continue our pursuit optimizing the inhibitors solubility and efficacy to meet the stringent criteria required for it to transition into a viable clinical candidate. As our preclinical results did not show efficacy of the BRN2i in multiple PDX models we have not pursued the development of clinical evaluation of this inhibitor.

Milestone #2: Co-author manuscripts on targeting BRN2 in preclinical models of AR-null CRPC, predictors of response and mechanisms of resistance.

We presented our findings through multiple oral and poster presentations:

Oral presentation as a visiting lecturer

1. Understanding Phenotypic Plasticity in Hormone Therapy Resistance. November 21st, 2022. Lady Davies Institute For Medical research, Regenerative Medicine Seminar, McGill University. Invited by Dr. Michael Witcher.
2. Lineage plasticity in hormone therapy resistance. Life Science Institute, UBC. June 3rd, 2022. Invited by Dr. Moukhles
3. Lineage plasticity in treatment resistance prostate cancer. University at Buffalo, CTSI Community of Scholars Seminars Series June 7th, 2022. Invited by Dr. Adelaiye-Ogala
4. Cell Plasticity in Treatment Prostate Cancer Resistance. Dana Farber Cancer Institute, Prostate Cancer SPORE Seminar (January 11th, 2022). Invited by Dr. Balk
5. Lineage Plasticity in Prostate Cancer Treatment Resistance. Cedars Sanai, BFG/Genomics Core Seminar Series, Los Angeles, CA (December 14th, 2021). Invited by Dr. Ellis
6. Lineage Plasticity in Prostate Cancer Treatment Resistance. UT Southwestern Hamon Center for Therapeutic Oncology Research & Simmons Comprehensive Cancer Center Experimental Therapeutics Program (October 7, 2021). Invited by Dr Raj
7. Cellular plasticity in treatment resistance prostate cancer. GU Oncology Lecture Series, Fred Hutch, Seattle (September 23, 2021). Invited by Dr. Nelson
8. Mechanisms of hormone therapy resistance in prostate cancer. PCF-UK, July 2021
9. Lineage plasticity as a mechanism of hormone therapy resistance in prostate cancer, Prostate Cancer Center of Excellence at Mount Sinai and the Tisch Cancer Institute, New York, NY, USA (February 3rd, 2021). Invited by Dr. Kyprianou
10. Cellular Plasticity in Prostate Cancer Treatment Resistance, Weill Cornell Medicine, New York, NY, USA (February 27, 2020). Invited by Dr. Rickman
11. Phenotypic Plasticity in treatment resistance, BC Cancer Agency, Vancouver, BC, Canada, (February 10, 2020). Invited by Dr. Krystal
12. Cellular plasticity in treatment resistant prostate cancer, Queens University, Ontario, Canada, (November 21, 2019) Invited by Dr. Koti
13. Tackling the new face of prostate cancer, Queens University, Ontario, Canada, (November 21, 2019) Invited by Dr. Koti
14. Cellular plasticity in treatment resistant prostate cancer, UC Davis, Sacramento, California, USA, (October 10, 2019) Invited by Dr. Ghosh
15. Cellular plasticity in treatment resistant prostate cancer, Cleveland Clinic, Cleveland, Ohio, USA, (October 2, 2019) Invited by Dr. Sharifi
16. AR switch in treatment resistance, The Vancouver Prostate Centre, UBC, Vancouver, BC, Canada

17. Cellular plasticity in treatment resistant prostate cancer, Princess Margaret Cancer Centre, University of Toronto, Toronto, ON, (April, 2019) Invited by Dr. He
18. Cellular plasticity in treatment resistant prostate cancer, Department of Cellular and Physiological Sciences, University of British Columbia, Vancouver, BC, Invited by Dr. Rideout
19. Hormone therapy induces reprogramming to drive aggressive prostate cancer, Centre Hospitalier Universite de Montreal (CHUM), Montreal (November 27, 2018), Invited by Dr. Mass-Masson
20. Cellular plasticity in treatment resistance prostate cancer, Institut de Recherche sur l'Immunologie et le Cancer (IRIC), Montreal (November 26, 2018), Invited by Dr. Mader
21. Cellular Plasticity and Neuroendocrine Phenotype in Prostate Cancer, US National Institute of Health/NCI, Bethesda (November 1st, 2018), Invited by Dr. Sowalsky
22. Cellular Plasticity in treatment resistance, Cedars Sinai & UCLA, Los Angeles, CA, USA (March 8, 2018), Invited by Dr. Freeman

Oral presentation at Conferences:

1. Cellular Plasticity and Neuroendocrine phenotype in Prostate Cancer. 25th European congress of Endocrinology (ECE 2023). 13-16 May, Istanbul Turkey. Conference Faculty invitee
2. Neuroendocrine Prostate Cancer. Prostate Cancer Academy. 18 April 2023, Netherland (virtual).
3. Novel Therapeutic Developments in Targeting the AR Pathway. 42nd Congress of the societe International d'Urologie. Montreal, Qc, Canada. November 9-13, 2022. Invited by Dr. Klotz
4. Studying NEPC, what are the best systems and what have we learnt by using them? EMBO Workshop: A 20/20 vision of the future of nuclear receptors. September 12 – 16, 2022 | Floriana, Malta. Invited by Dr. Carroll
5. Activation of Neuronal Lineage Programs to Bypass Androgen Signaling Inhibition in Prostate Cancer. ENDO2022 Atlanta, Georgia (June 13, 2022). Invited by Dr. Frigo
6. The role of AR in lineage plasticity. 3rd Annual conference on nuclear receptors. Cancun (May 4-7, 2022). Invited by Dr. Beavan
7. Understanding and targeting cell plasticity in treatment resistance prostate cancer. Pfizer, Lajolla (January, 2022). Invited by Dr. Davies
8. Things I learned during my scientific journey. Young Investigator Day, 28th Prostate Cancer Foundation Annual Retreat (October 22, 2021), Virtual meeting, Invited by Dr. Soule
9. Targeting Neuroendocrine transformed cells to overcome treatment resistance. 27th Prostate Cancer Foundation Annual Retreat (October 28, 2021), Virtual meeting, Invited by Dr. Armstrong
10. From target identification, validation to drug discovery. Annual Scientific meeting, Tetouan, Morocco (July 5th, 2020), Virtual Meeting, Invited by Dr. kandouz
11. AR switch in treatment resistance, 7th Coffey Holden Prostate Cancer Academy, Los Angeles, CA, USA (June 20-23, 2018). Invited by Dr Soule
12. Cell plasticity in treatment resistant prostate cancer, 7th International PacRim Breast & Prostate Cancer Meeting (17-20 March, 2019) Barossa Valley, South Australia, Australia, Invited by Dr Tilley.
13. Androgen Receptor Switch in treatment resistant prostate cancer. 3rd workshop on Reducing the Burden of bone metastatic prostate cancer (February, 2019), La Jolla, CA, USA. Invited by Dr. Jamieson
14. Hormone therapy induces reprogramming to drive aggressive prostate cancer. 1st Workshop on cellular plasticity in androgen independent prostate cancer, US National Institute of Health. Bethesda, Maryland, USA (December 6-7, 2018). Invited by Dr. Beltran
15. Cellular Plasticity and the Neuroendocrine Phenotype in Prostate Cancer. The 25th Scientific Retreat, Prostate Cancer Foundation. Carlsbad, California, USA (Oct 25-28, 2018). Invited by Dr Soule
16. Targeting the AR regulated gene BRN2 in neuroendocrine prostate cancer. EMBO Workshop on Nuclear Receptors. Kolymbari, Crete, Greece (Sept 11-15, 2018).
17. Cellular Plasticity in Treatment Resistance. Coffey Holden Prostate Cancer Academy, Los Angeles, CA, USA (June 21-24, 2018). Invited by Dr Carlo

Title – "Selective inhibition of transcription factor BRN2 as a treatment strategy for Small Cell Prostate Cancer" Thaper D, Munuganti R, Aguda A, Ku S, Kumar S, Kim S, Vahid S, Sivak O, Puca L, Bishop JL, Morrissey C, Corey E, Beltran H and Zoubeidi A

1. Poster presentation at AACR Virtual Annual Meeting II (2020)

2. Invited Talk at AACR Advances in Prostate Cancer Research (2020), Denver, CO, USA *cancelled due to COVID19*
3. Poster presentation at Prostate Cancer Foundation Annual Retreat (2019), Carlsbad, CA, USA (2019)
4. Poster presentation at the FEBS Workshop: Nuclear Receptors, Spetses Island, Greece (2019)

Furthermore, we have taken steps to disseminate our work to a broader audience by publishing part of our findings on bioRxiv, a platform that facilitates early access to cutting-edge research.

Title – "Discovery and characterization of a first-in-field transcription factor BRN2 inhibitor for the treatment of neuroendocrine prostate cancer.
Thaper D, Munuganti R, Aguda A, Kim S, Ku S, Sivak O, Kumar S, Vahid S, Ganguli D, Beltran H, Morrissey C, Corey E and Zoubeidi A
bioRxiv preprint doi: https://doi.org/10.1101/2022.05.04.490172

SPECIFIC AIM 3: DEVELOPMENT OF IGFBP2 AND IGFBP5 AS COMPANION DIAGNOSTIC MARKERS FOR GUIDED PATIENT SELECTION.

Subtask 1: Measure serum levels of NPTX1 in the NEPC PDX models during treatments suggested in Aim 2. Zoubeidi, Corey, Morrissey

For this aim, our goal was to validate IGFBP5 as a pharmacodynamics marker for BRN2 activity as well as explore its potential as a marker for NE-trans-differentiation. We purchased over five different commercially available ELISA kits including some that were used in previous publications and some that were not. Unfortunately, all the kits failed to detect IGFBP5 efficiently; while they were able to detect positive control peptide, all the kits failed negative controls and demonstrated strong non-specific binding. We developed and optimized an assay in year 2 as indicated in our previous report. However, this IGFBP5 antibody lot is not available anymore and again we couldn't detect IGFBP5 in the serum.

Faced with these challenges we took a more comprehensive approach to identify another BRN2 serum marker. We analyzed new data generated in our labs and public data sets and used different approaches, and identified and validated NPTX1 as a serum marker for BRN2 expression/activity. Next, we evaluated patient's serum samples and were able to detect NPTX1 in the serum of NEPC patients (details below). To identify candidate serum biomarkers of $BRN2^{+}$ NEPC, we followed the workflow shown in Fig. 16A. We performed chromatin immunoprecipitation (ChIP) followed by sequencing (ChIP-seq) to identify sites of chromatin-bound BRN2 in the NEPC cell lines NCI-H660 and $42D^{ENZR}$. MACS2[62] was used to identify peaks (genomic regions where the ChIP target protein, in this case BRN2, is enriched compared to background) in ChIP-seq data. We analyzed BRN2 ChIP-seq peak sets from two independent NCI-H660 samples and one $42D^{ENZR}$ sample and identified a total of 5,166 peaks that were shared by at least two of the three peak sets. We then annotated these shared peaks with nearby genes using UROPA[59]. Specifically, we identified all genes within 20 kb of a BRN2 peak. We additionally, located all peaks that overlapped any enhancer in the EnhancerAtlas 2.0 database having known regulatory links to genes (in any human cell type). All genes linked to enhancers overlapped by BRN2 peaks were subsequently included in our peak annotation. We considered the complete list of genes annotated to peaks (12,924 genes) to be genes that are potentially regulated by BRN2 in NEPC. Because we were specifically interested in finding a serum biomarker for $BRN2^{+}$ NEPC, we then filtered the list of potential BRN2 target genes to retain only genes that encode secreted proteins listed in the Human Protein Atlas secretome database. This resulted in 507 candidate genes for a serum biomarker.

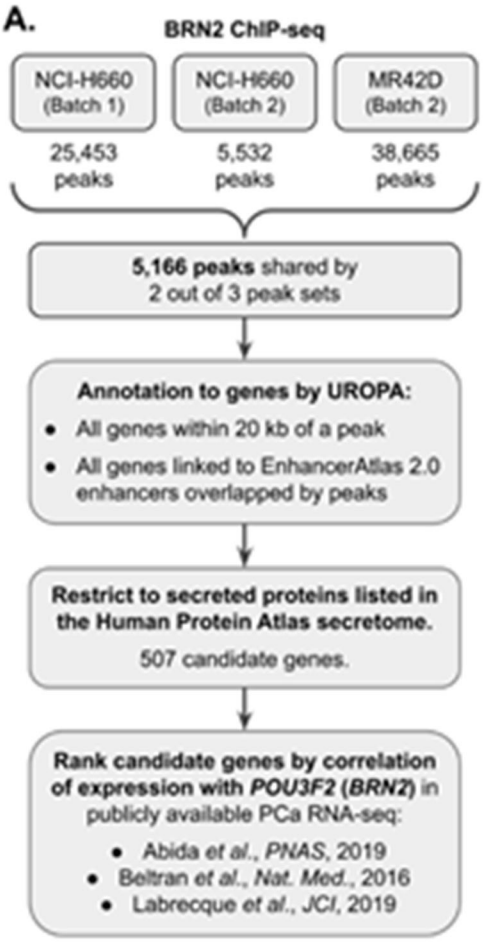

B.

Gene	ρ (Abida 2019, polyA)	ρ (Abida 2019, capture)	ρ (Labrecque 2019)	ρ (Beltran 2016)	Combined p-value	BH-adjusted combined p-value
NCAN	0.38	0.46	0.48	0.44	1.60E-27	7.94E-25
NPTX1	**0.31**	**0.42**	**0.39**	**0.64**	**1.53E-23**	**3.79E-21**
NTN3	0.23	0.45	0.53	0.45	5.02E-23	8.32E-21
RTBDN	0.30	0.38	0.50	0.49	1.26E-21	1.56E-19
LCN15	0.29	0.46	0.34	0.50	2.25E-21	2.24E-19
BTBD17	0.25	0.45	0.30	0.55	4.77E-20	3.95E-18
DAND5	0.19	0.40	0.49	0.55	1.02E-19	7.27E-18
C14orf93	0.27	0.39	0.36	0.58	4.12E-19	2.56E-17
INHBE	0.28	0.42	0.32	0.42	6.02E-18	3.32E-16
FBN3	0.25	0.45	0.32	0.31	2.68E-17	1.33E-15

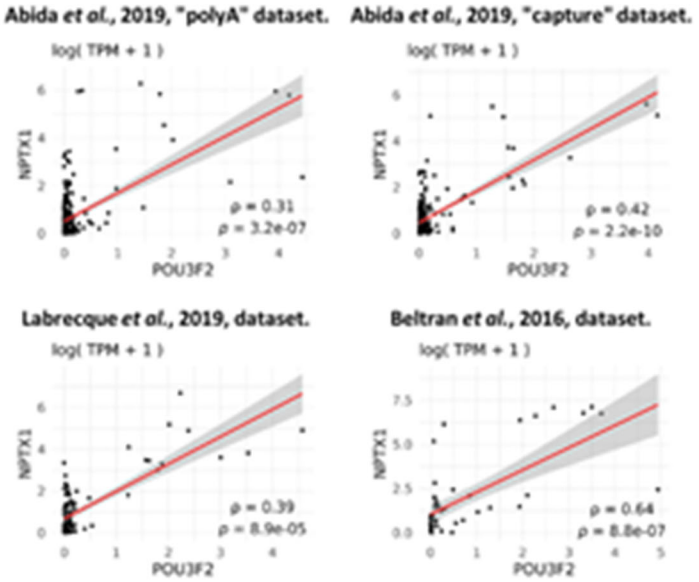

Figure 16: Identification of NPTX1 as a candidate serum biomarker for BRN2⁺ NEPC. A. Analysis workflow to identify and prioritize potential serum biomarkers of BRN2⁺ NEPC. Figure 1: **B.** Top: Spearman correlations, *ρ*, of mRNA expression of the top 10 serum biomarker candidates with *POU3F2* expression in four publicly available PCa RNA-seq datasets. The p-values were combined for each gene using Fisher's method, and adjusted for multiple hypothesis testing using the Benjamini-Hochberg procedure. Genes were ranked from most significant combined p-value to least significant. Bottom: scatter plots of *NPTX1* vs *POU3F2* mRNA expression in the four RNA-seq datasets. Linear trend lines are shown (red lines) with their 95% confidence intervals (shaded areas

To prioritize candidate genes for investigation, we ranked the 507 candidate genes by their correlations with BRN2 mRNA (*POU3F2*) expression in PCa patient specimens in publicly available RNA-seq datasets (Fig. 16B). For this, we used RNA-seq data from studies by Abida *et al.*[60], Labrecque *et al.*[8], and Beltran *et al.*[61]. The study by Abida *et al.* used two different RNA-seq methods – enrichment for polyadenylated RNA and exon capture – which we treated as two separate datasets, labeled "polyA" and "capture" respectively. In each of the four RNA-seq datasets, we computed the Spearman correlation, ρ, of each candidate gene with *POU3F2*. We combined the p-values associated with the four correlation coefficients for each gene using Fisher's method and subsequently ranked the genes from most significant to least significant correlation. Neuronal pentraxin 1 (NPTX1) ranked second in this analysis, but its detected gene expression values (TPM values) were substantially higher than the top-ranked gene, NCAN, in *POU3F2*-high patients (Fig. 17), an important consideration for detection of the protein in serum.

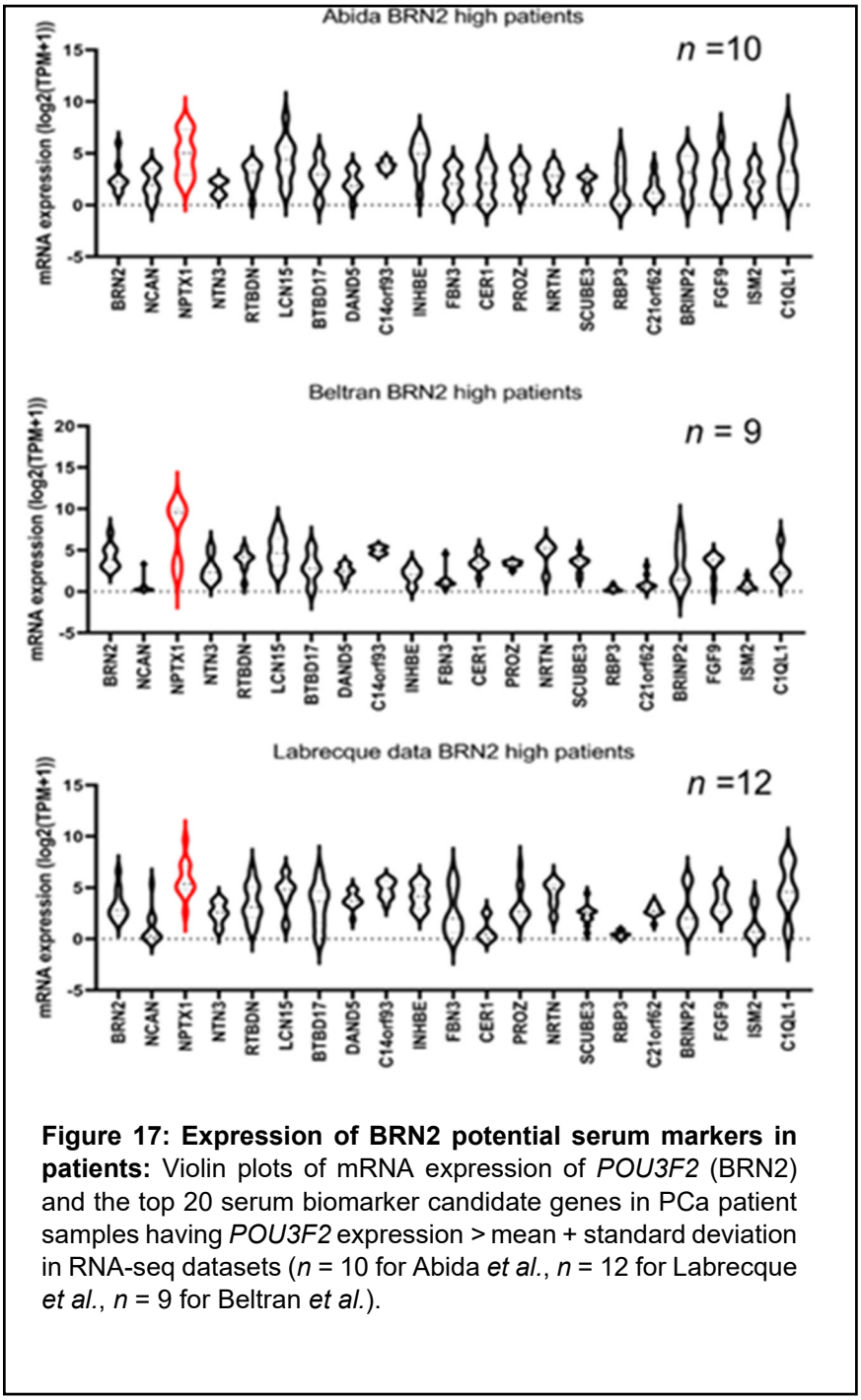

Figure 17: Expression of BRN2 potential serum markers in patients: Violin plots of mRNA expression of *POU3F2* (BRN2) and the top 20 serum biomarker candidate genes in PCa patient samples having *POU3F2* expression > mean + standard deviation in RNA-seq datasets (n = 10 for Abida *et al.*, n = 12 for Labrecque *et al.*, n = 9 for Beltran *et al.*).

Subtask 2: Utilizing CRPC PDX lines or cell lines, examine the kinetics of IGFBP2 and IGFBP5 serum levels vs PSA during acquisition of ENZ resistance.

Zoubeidi, Corey, Morrissey

We also looked at the expression of NPTX1 in LTL331 PDX models[28] that develop NEPC post castration (Fig. 18A) and observed an increase in the expression of BRN2 (Fig. 18B) and NPTX1 (Fig. 18C) in NEPC. Accordingly, expression of PSA correlated negatively with BRN2 and NTX1 and was downregulated in NEPC (Fig. 18D).

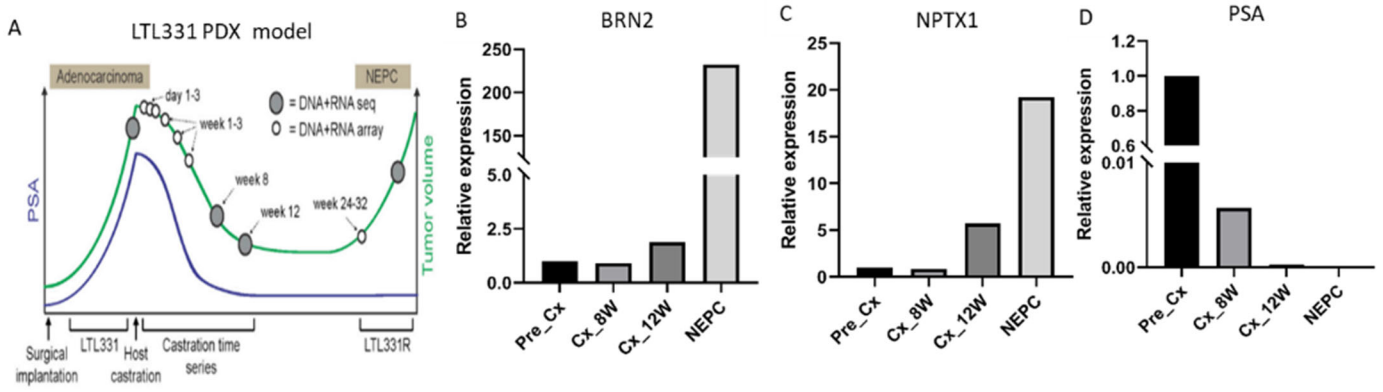

Figure 18: A) Schematic present generation of LTL331 PDX model. Relative mRNA expression normalized to pre-castration (pre-CX) showing expression of **B)** BRN2 **C)** NPTX1 **D)** PSA

Interrogation of our BRN2 ChIP-seq data confirmed the presence of a robust BRN2 peak downstream of the *NPTX1* gene in both, NCI-H660 and 42D^{ENZR} cell lines (Fig. 19, left). This peak coincided with marks of an active promoter element (H3K27ac and H3K3me3; Fig. 19, left) and in fact resided in the promoter of a long non-coding RNA (lncRNA) gene. H3K4me3 was also observed at the *NPTX1* promoter in both NCI-H660 and 42D^{ENZR}, as was H3K27ac in NCI-H660 (Fig. 19, left). Intriguingly, the lncRNA promoter element was also highly active in 16D^{CRPC}, a PCa cell line that represents an earlier stage of the disease and does not express BRN2.

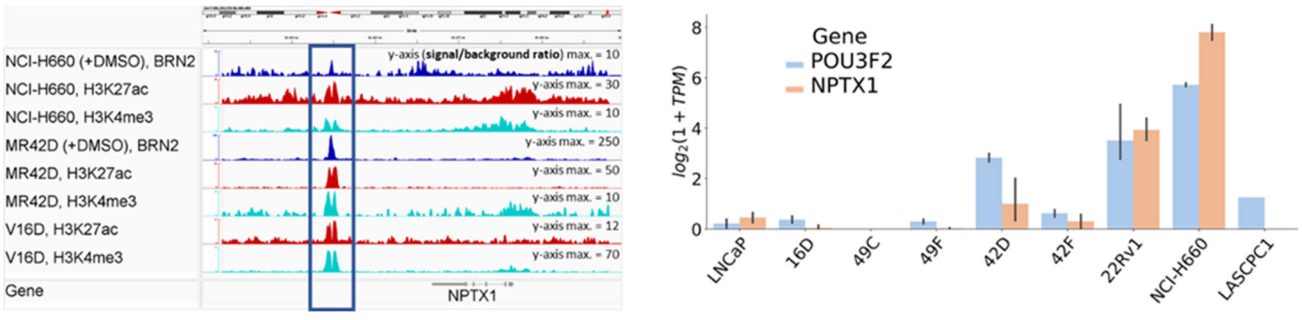

Figure 19: Left panel: ChIP-seq tracks for BRN2, H3K27ac, and H3K4me3 around the *NPTX1* locus in NCI-H660 and MR42D cells, and for H3K27ac and H3K4me3 in V16D cells. The *y*-axis shows the ratio of ChIP signal to background. **Right panel** *POU3F2* and *NPTX1* gene expression from RNA-seq data for nine PCa cell lines: LNCaP (*n* = 2), V16D (16D; *n* = 3), 49C (*n* = 1), 49F (*n* = 2), MR42D (42D; *n* = 9), 42F (*n* = 2), 22Rv1 (*n* = 3), NCI-H660 (*n* = 2), and LASPC1 (*n* = 1). Bar heights show mean expression values, error bars show 95% confidence intervals.

Nevertheless, across RNA-seq data from nine PCa cell lines, *NPTX1* expression was high only in cell lines that highly expressed *POU3F2* (Fig. 19, right). Furthermore, we recently found by Western blot that overexpression of BRN2 in 22Rv1 cells, which already express both BRN2 and NPTX1, increases the protein levels of NPTX1. Considering all of these data, we hypothesize that recruitment of BRN2 to an already active cis-regulatory element, the promoter of a lncRNA gene, causes upregulation of the nearby *NPTX1* gene.

To further evaluate *NPTX1* regulation by BRN2, we downloaded publicly available BRN2 ChIP-seq data for LK2 and NCI-H520, two lung squamous cell carcinoma (LUSC) cell lines of a neural subtype defined by BRN2 and SOX2[16], and performed a refined version of our analysis workflow shown in Fig 1. Using the peaks in the higher-quality of our two NCI-H660 BRN2 ChIP-seq samples, plus the BRN2 peak sets from 42D^{ENZR}, LK2, and NCI-H520, we identified 493 BRN2 peaks that were shared by at least three out of four peak sets. We then refined the first step of our peak annotation strategy to reduce the average number of genes per peak by annotating peaks in promoters of known protein-coding genes only to genes corresponding to those promoters, rather than all genes within 20 kb (annotation of all other peaks remained unchanged). Applying this refined analysis to the new set of 493 BRN2 peaks, and filtering the gene list to retain only secreted proteins resulted in identification of 51 genes. This list includes *NPTX1*, as the BRN2 peak downstream of *NPTX1* in NCIH660 and MR42D cells as well as in both the LK2 and NCI-H520 cell lines (Fig. 20), even though only 302 non-blacklisted BRN2 peaks were detected in NCI-H520. After ranking the 51 BRN2 serum biomarker candidates, NPTX1 ranked as a top candidate (NCAN was lost from the list of candidates and no stronger candidates were gained), thus increasing our confidence in NPTX1 as the most promising candidate for a serum biomarker of BRN2^{+} NEPC.

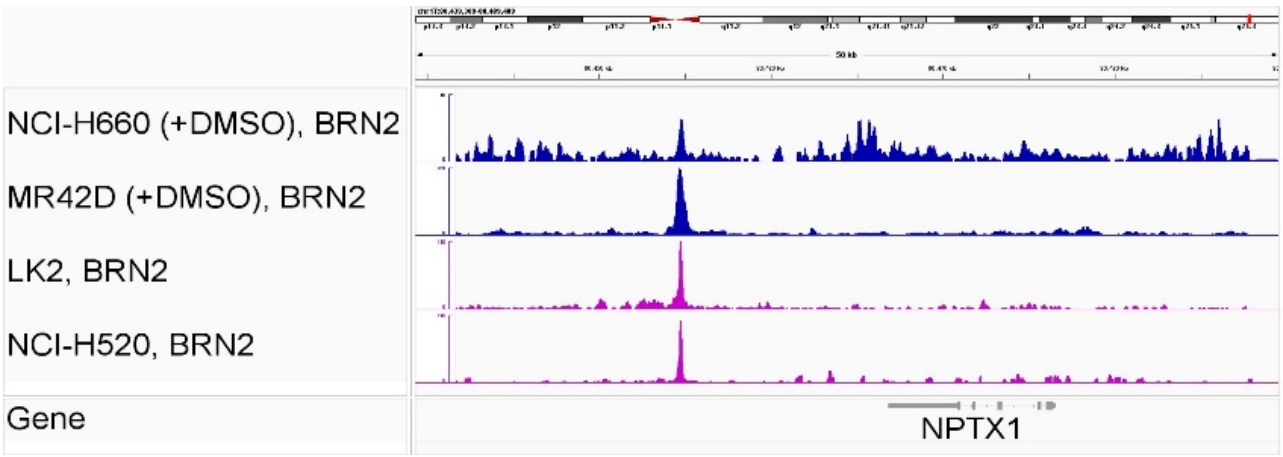

Figure 20: BRN2 ChIP-seq tracks around NPTX1 in the NEPC cell lines NCI-H660 and 42D^{ENZR} and the neural-type LUSC cell lines LK2 and NCI-H520.

To test whether NPTX1 protein is secreted by cells at a detectable level, we performed Western blots using either cell lysate or culture media from NCI-H660 cells. As anticipated, we detected NPTX1 from both cell lysate and media, whereas BRN2 was only detected only in cell lysate (Fig. 21A). Using a commercially available ELISA Kit (R-PLEX Human NPTX1 Assay), we validated the presence of NPTX1 in culture media (Fig. 21B).

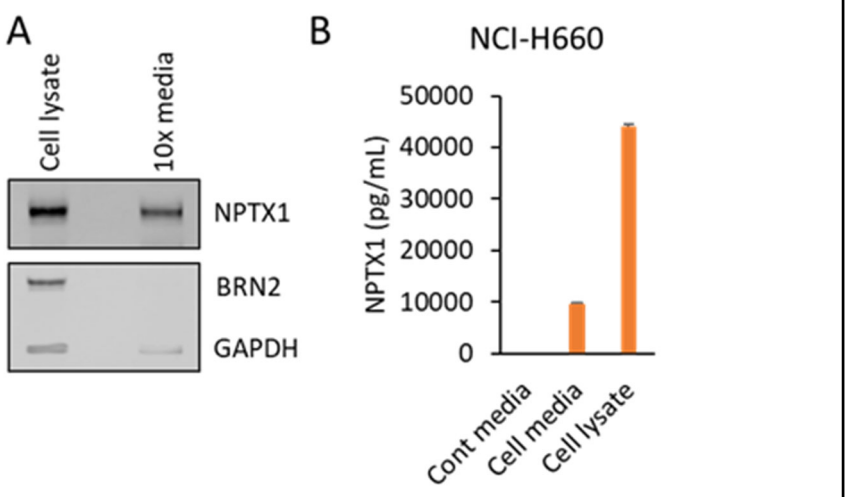

Figure 21: Expression of NPTX1 in the media of NCI-H660 cells. A) Western blots for NPTX1 and BRN2 from either cell lysate or culture media from cultured NCI-H660 cells. **B)** level of NPTX1 detected by R-PLEX Human NPTX1 Assay kit in control media, NCI-H660 cultured media, and NCI-H660 cell lysate

Next, we performed an *in-vivo* experiment and collected the serum from mice bearing NCI-H660 xenografts over time. Our data showed that NPTX1 is present in the serum and that serum NPTX1 levels increased as NCI-H660 xenograft tumors increased in volume (Fig. 22).

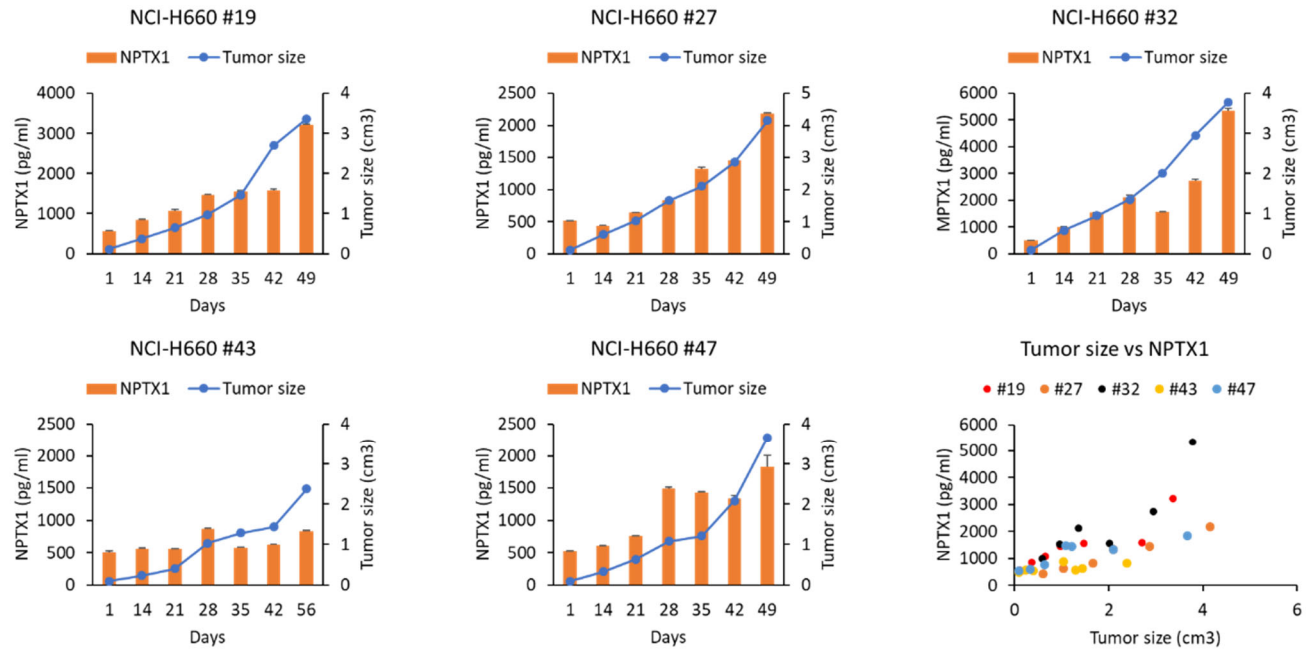

Figure 22: **Serum NPTX1 levels *in vivo*.** NCI-H660 cells were injected subcutaneously into mice and serum from mice was collected over time. NPTX1 was measured using ELISA Kit (R-PLEX Human NPTX1 Assay). NPTX1 correlates with tumor volume.

In search of more support for NPTX1 as a serum biomarker for BRN2 activity, we investigated expression of *POU3F2* and *NPTX1* in prostate cancer publicly available scRNA-seq data[1]. Overlaying *POU3F2* and *NPTX1*, as well as *ASCL1*, expression on a UMAP visualization of the scRNA-seq data showed that *NPTX1* expression was most evident in the two patients that clearly expressed *POU3F2*, one of whom had adeno histology and did not express *ASCL1*, which is a master regulator of many neuroendocrine tumors and may also positively regulate *NPTX1* expression (Fig. 23). The highest *NPTX1* expression was in a patient that co-expressed *POU3F2* and *ASCL1*. Some *NPTX1* expression could also be observed in one *ASCL1+ POU3F2-* tumor but not in another patient who had both *ASCL1+ NEUROD1- POU3F2-* and *ASCL1- NEUROD1+ POU3F2-* populations. These data suggest that, *NPTX1* is associated more with *POU3F2*-expressing tumors than with the general neuroendocrine phenotype.

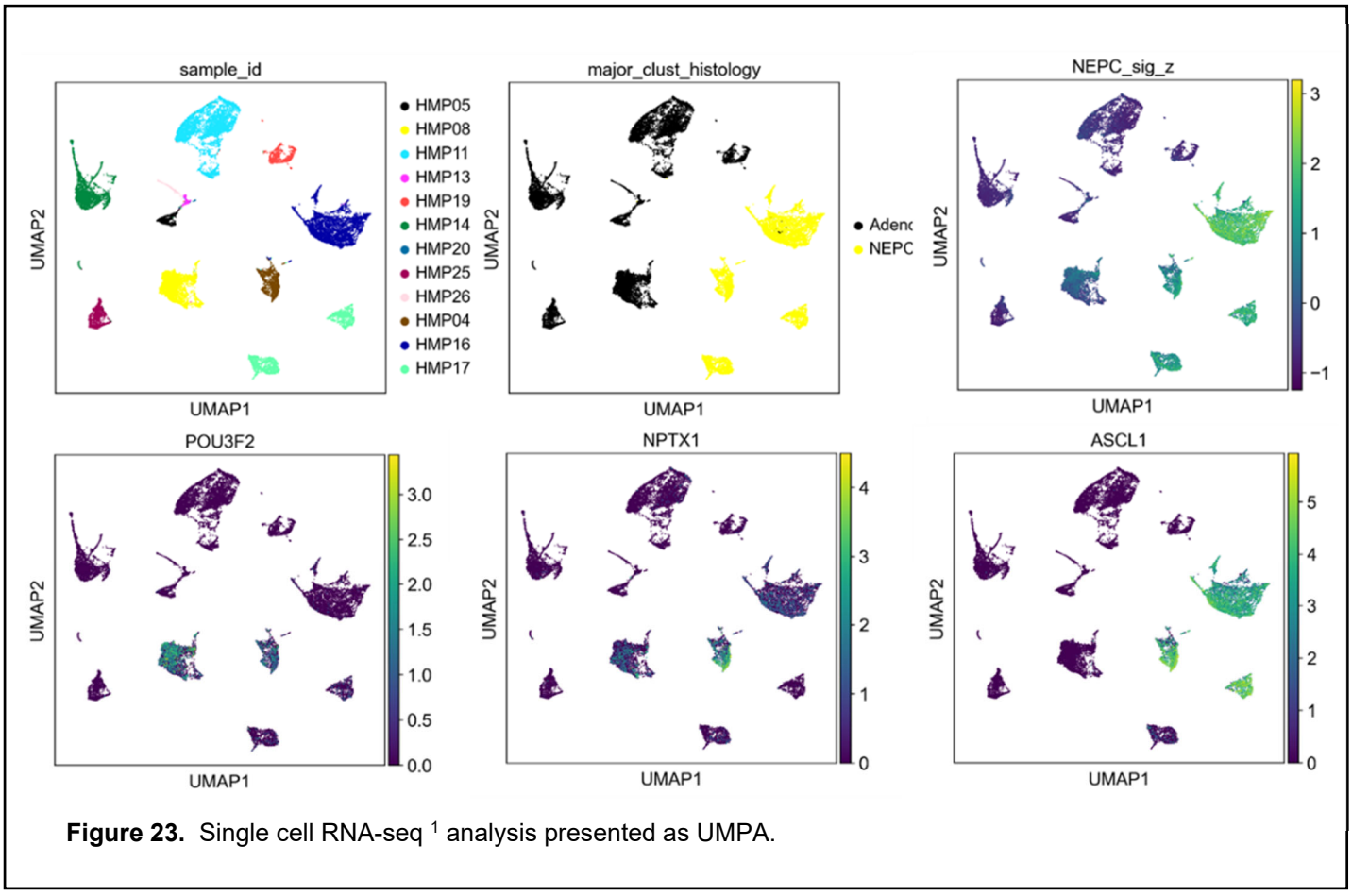

Figure 23. Single cell RNA-seq [1] analysis presented as UMPA.

To gain more insight into the potential importance of BRN2 in the wider regulation of *NPTX1*, we fitted linear models of *NPTX1* expression to the expression of several potential upstream regulators in the scRNA-seq data. To reduce both data sparsity and pseudoreplication bias (the statistically incorrect treatment of multiple cells in the same state as biological replicates), we aggregated similar cells from the same patient into small clusters of cells called “metacells” (containing ~75 cells each or otherwise up to a maximum of 50 metacells per patient) using the SEACells method[63] (DOI: 10.1038/s41587-023-01716-9). We then obtained a list of potential regulators of *NPTX1* from the Toolkit for Cistrome DB (http://dbtoolkit.cistrome.org/), keeping transcription factors (TFs) with regulatory potential > 0.6 at a half-decay distance of 1 kb or 10 kb. Since c-Myc and MAX were in this list, we also added N-Myc and L-Myc (L-Myc is absent from Cistrome DB due to lack of ChIP-seq data). Adding BRN2 to this list, we eventually considered the following potential regulators of *NPTX1*: POU3F2, ASCL1, RNF2, RUNX1, ZNF467, ESR1, EGR3, SNAI2, MYC, MYCN, MYCL, MAX, IRF4, OTX2, SMAD3, SPI1, and GLIS1.

We then performed a non-negative least squares (NNLS) linear regression with zero intercept to model *NPTX1* expression in the metacells as a linear combination of the expression levels of these genes, allowing the model to also consider library size and metacell size as confounding variables (an initial NNLS fit with nonzero intercept yielded an undesirable negative intercept term, so we refitted the model without an intercept term). This regression yielded the following model (coefficients are standardized) with an R^2 score of 0.636: *NPTX1* = 0.467**MYCL* + 0.212**MYCN* + 0.125**ASCL1* + 0.124**POU3F2*.

To gain more insight into the potential importance of BRN2 in the wider regulation of *NPTX1*, we fitted linear models of *NPTX1* expression to the expression of several potential upstream regulators in the scRNA-seq data. To reduce both data sparsity and pseudoreplication bias (the statistically incorrect treatment of multiple cells in the same state as biological replicates), we aggregated similar cells from the same patient into small clusters of cells called "metacells" (containing ~75 cells each or otherwise up to a maximum of 50 metacells per patient) using the SEACells method[63] (DOI: 10.1038/s41587-023-01716-9). We then obtained a list of potential regulators of *NPTX1* from the Toolkit for Cistrome DB (http://dbtoolkit.cistrome.org/), keeping transcription factors (TFs) with regulatory potential > 0.6 at a half-decay distance of 1 kb or 10 kb. Since c-Myc and MAX were in this list, we also added N-Myc and L-Myc (L-Myc is absent from Cistrome DB due to lack of ChIP-seq data). Adding BRN2 to this list, we eventually considered the following potential regulators of *NPTX1*: POU3F2, ASCL1, RNF2, RUNX1, ZNF467, ESR1, EGR3, SNAI2, MYC, MYCN, MYCL, MAX, IRF4, OTX2, SMAD3, SPI1, and GLIS1. We then performed a non-negative least squares (NNLS) linear regression with zero intercept to model *NPTX1* expression in the metacells as a linear combination of the expression levels of these genes, allowing the model to also consider library size and metacell size as confounding variables (an initial NNLS fit with nonzero intercept yielded an undesirable negative intercept term, so we refitted the model without an intercept term). This regression yielded the following model (coefficients are standardized) with an R^2 score of 0.636: *NPTX1* = 0.467**MYCL* + 0.212**MYCN* + 0.125**ASCL1* + 0.124**POU3F2*.

A 5-fold cross-validated elastic net with zero intercept and non-negative constraint on coefficients selected the same 4 terms for the model with only modestly different coefficients.

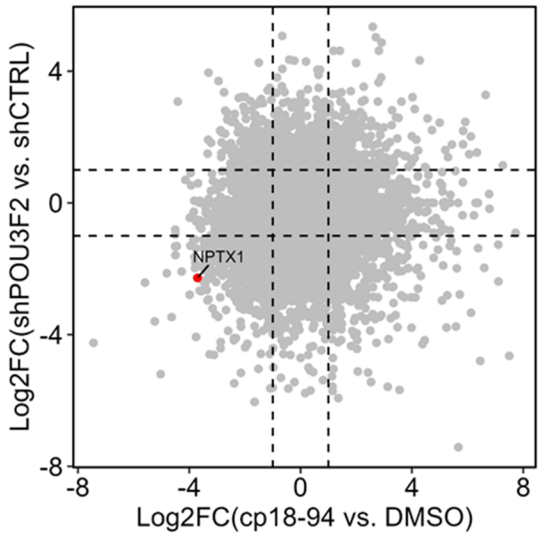

Figure 24. Comparing NEPC *cell line* (42D^{ENZR}) shBRN2 to shCTL (y axis) as well as treated with BRN2i (18-94) for 72 hours compared to DMSO. Data is presented as log2FC, with each dot representing one gene. Dashed line is presenting the p-value of 0.05. NPTX1 shown as red dot.

To allow for the possibility that a target gene requires TFs to work together for regulation, we then added all pairwise interactions of the above four genes to the model, used another 5-fold cross-validated elastic net to select the most informative interaction terms, and then refitted the model with the above four genes and the selected interaction terms using NNLS with zero intercept. This resulted in the following fitted model with R^2 = 0.807: *NPTX1* = 0.146**POU3F2* + 0.002**MYCN* + 0.274**ASCL1***MYCL* + 0.040**POU3F2***MYCL* + 0.009**ASCL1***MYCN* + 0.027*metacell-size.

These results indicate that, although *POU3F2* expression is not necessarily the strongest predictor of *NPTX1* expression, it is nevertheless an important predictor. Notably, even with the allowance of pairwise interaction terms in the linear model, *POU3F2* was still selected as an important main effect, suggesting that other TFs and their interactions are not sufficient to fully explain *NPTX1* expression without BRN2.

We observed NPTX1 to be downregulated in NEPC shBRN2 compared to shCTL as well as in NEPC treated with BRN2i compared to DMSO (Fig. 24). Together our results support our hypothesis that NPTX1 is a suitable serum biomarker for BRN2+ NEPC, but more samples will need to be analyzed before conclusions can be drawn.

Subtask 3: Validate the findings from the PDX in serum samples of patients undergoing anti-androgen therapies.

Zoubeidi, Morrissey

Having verified NPTX1 in culture media from NCI-H660 cells and serum from mice with NCI-H660 xenograft tumors, we next evaluated serum from LuCaP PDX models. We observed strong positive correlation between NPTX1 levels and mRNA NPTX1 expression multiplied tumor volume (r=0.96) (Fig. 25A). Finally, we measured serum NPTX1 level in samples from patients with metastatic PCa from the University of Washington under the Prostate Cancer Donor Program. Overall, serum NPTX1 levels were correlated with tumor NPTX1 mRNA expression in same patients (r=0.56) (Fig. 25B). Although we observed a positive correlation between POU3F2 and NPTX1 mRNA expression in patients' tumor (r=0.69), we observed a weak positive correlation between BRN2 mRNA expression in tumors and serum NPTX1 (r=0.22). We hypothesize that this is due to the end-stage patients having multiple metastasis and tumor heterogeneity.

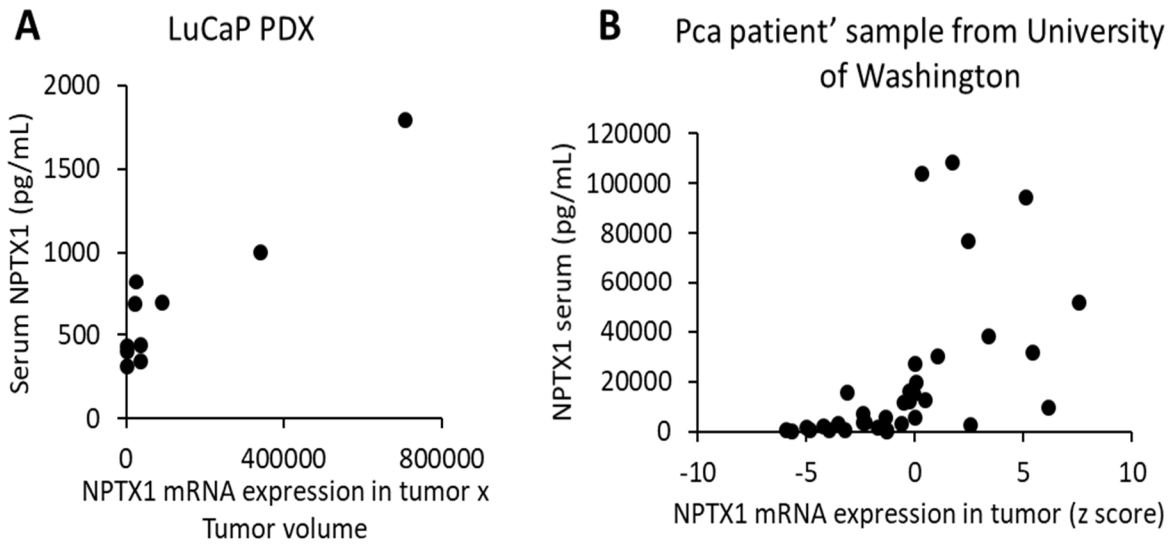

Figure 25: **A)** Correlation between serum NPTX1 level and NPTX1 mRNA expression in tumor multiplied tumor volume in LuCaP PDX models. **B)** Correlation between serum NPTX1 level and NPTX1 mRNA expression in human prostate cancer tissue. Tissue RNA-seq data (acquired after rapid autopsy) and serum from the corresponding patients were provided by the University of Washington under the Prostate Cancer Donor Program.

Our investigation yielded compelling results, as we observed a converse correlation between the levels of PSA and NPTX1 in PCa xenograft models (Fig. 18). To further investigate this observation, we used the DRANA study cohort[64]. We observed that patients post 3 months of enzalutamide treatment show significant reduction of PSA, while a subset of patients also show a significant increase of NPTX1 expression (Fig. 26). This convergence of evidence underscores the clinical relevance of our findings and reinforces the potential utility of NPTX1 as a valuable biomarker for PCa management and monitoring, particularly in the context of anti-androgen therapies.

Validating our observation in clinical samples represents a pivotal aspect of our study, and we are committed to conducting it with the utmost scientific rigor to ensure the robustness and reliability of our findings.

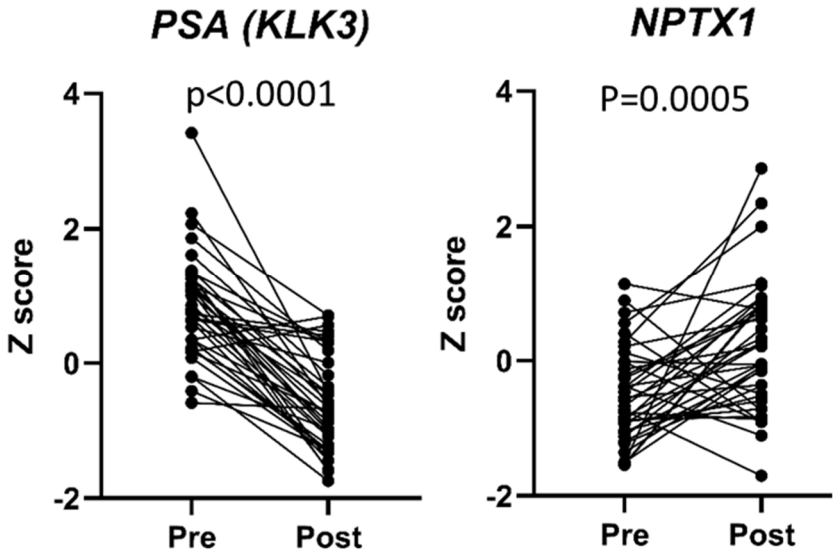

Figure 26: KLK3, and NPTX1 mRNA expression in DARANA study cohort. Each dot shows NPTX1 expression in pre and post-Enzalutamide treatment patients Pair t-test

Subtask 4: Discuss the development of clinical trial concepts with institutional physicians based on positive preclinical results.

Zoubeidi, Corey, Morrissey

It is notable that, despite the promising preclinical outcomes, our lead inhibitor remains under active development. We are dedicated to the refinement and optimization of this inhibitor to meet the stringent criteria essential for it to be considered a viable clinical candidate.

Milestone #3: Incorporation of NPTX1 within the BRN2i PDX manuscript.

We are actively engaged in assessing the safety and efficacy of our lead inhibitor within *in vivo* settings. Once we proceed with the BRN2i PDX manuscript we will insure integrating our findings regarding NPTX1 in it.

Conclusion

BRN2 functions as a pioneer factor in NEPC: In NEPC 42D^{ENZR} model, BRN2 binds to both open and closed regions of chromatin. Moreover, the BRN2 cistrome is primarily linked to the transcriptionally active genes as 81% of H3K4me3 and H3K27Ac (Hyper-active) and 81% of H3K4me3 and H3K27me3 (Bivalent) genomic loci are co-occupied by BRN2. Importantly, these exact genes/pathways are simultaneously downregulated by BRN2 knockout or inhibition via small molecule. Inhibition of BRN2 in NEPC resulted in increase chromatin accessibility associated with neuronal, stemness and proliferation programs, which were lost following this inhibition. Inversely, overexpression of BRN2 in CRPC model 16D^{CRPC} resulted in significant remodeling of chromatin with approximately closing of 60,000 regions. Investigating this further, we observed these regions to be enriched with motif of other neuronal transcription factors such as ASCL1 and LHX and associated with neuronal pathways. Altogether, support the important role of BRN2 in influencing the chromatin architecture to support the neuronal phenotype.

BRN2 score: Using 5 BRN2 ChIP-seqs combined with correlation studies using public RNA-seq data, we developed and validated 2 BRN2 scores (positively and negatively correlated with BRN2 activity) to be used to measure and segregate samples based on BRN2 activity.

NPTX1 as a marker for BRN2 activity and NE-differentiation: Through rigorous computational analysis of ChIP-seq and RNA-seq data sets, we identified NPTX1 as the strongest candidate as a serum biomarker of BRN2+ NEPC. We have also validated that NPTX1 is present in serum from patients with NEPC, but not BRN2− adenocarcinoma CRPC patients. Furthermore, upon BRN2 inhibition in tNEPC model, either using small molecule or shRNA, inhibition of BRN2 reduces NPTX1 mRNA and subsequent protein production and secretion as measurable by qPCR, WB and ELISA.

Inventions, Patents and Licenses

None

References

1. Chan, J.M. *et al.* Lineage plasticity in prostate cancer depends on JAK/STAT inflammatory signaling. *Science* **377**, 1180-1191 (2022).
2. Boumahdi, S. & de Sauvage, F.J. The great escape: tumour cell plasticity in resistance to targeted therapy. *Nat Rev Drug Discov* **19**, 39-56 (2020).
3. Davies, A.H., Beltran, H. & Zoubeidi, A. Cellular plasticity and the neuroendocrine phenotype in prostate cancer. *Nat Rev Urol* **15**, 271-286 (2018).
4. Scher, H.I. *et al.* Increased survival with enzalutamide in prostate cancer after chemotherapy. *N Engl J Med* **367**, 1187-1197 (2012).
5. de Bono, J.S. *et al.* Abiraterone and increased survival in metastatic prostate cancer. *N Engl J Med* **364**, 1995-2005 (2011).
6. Koshkin, V.S. & Small, E.J. Apalutamide in the treatment of castrate-resistant prostate cancer: evidence from clinical trials. *Ther Adv Urol* **10**, 445-454 (2018).
7. Aggarwal, R. *et al.* Clinical and Genomic Characterization of Treatment-Emergent Small-Cell Neuroendocrine Prostate Cancer: A Multi-institutional Prospective Study. *J Clin Oncol* **36**, 2492-2503 (2018).
8. Labrecque, M.P. *et al.* Molecular profiling stratifies diverse phenotypes of treatment-refractory metastatic castration-resistant prostate cancer. *J Clin Invest* **129**, 4492-4505 (2019).
9. Nouruzi, S. *et al.* ASCL1 activates neuronal stem cell-like lineage programming through remodeling of the chromatin landscape in prostate cancer. *Nat Commun* **13**, 2282 (2022).
10. Davies, A. *et al.* An androgen receptor switch underlies lineage infidelity in treatment-resistant prostate cancer. *Nat Cell Biol* **23**, 1023-1034 (2021).
11. Baca, S.C. *et al.* Reprogramming of the FOXA1 cistrome in treatment-emergent neuroendocrine prostate cancer. *Nat Commun* **12**, 1979 (2021).
12. Park, J.W. *et al.* Reprogramming normal human epithelial tissues to a common, lethal neuroendocrine cancer lineage. *Science* **362**, 91-95 (2018).
13. Cejas, P. *et al.* Subtype heterogeneity and epigenetic convergence in neuroendocrine prostate cancer. *Nat Commun* **12**, 5775 (2021).
14. Bishop, J.L. *et al.* The Master Neural Transcription Factor BRN2 Is an Androgen Receptor-Suppressed Driver of Neuroendocrine Differentiation in Prostate Cancer. *Cancer Discov* **7**, 54-71 (2017).
15. Robertson, A.G. *et al.* Comprehensive Molecular Characterization of Muscle-Invasive Bladder Cancer. *Cell* **171**, 540-556 e525 (2017).
16. Sato, T. *et al.* Epigenomic Profiling Discovers Trans-lineage SOX2 Partnerships Driving Tumor Heterogeneity in Lung Squamous Cell Carcinoma. *Cancer Res* **79**, 6084-6100 (2019).
17. Ishii, J. *et al.* POU domain transcription factor BRN2 is crucial for expression of ASCL1, ND1 and neuroendocrine marker molecules and cell growth in small cell lung cancer. *Pathol Int* **63**, 158-168 (2013).
18. Alvarez-Bolado, G. Development of neuroendocrine neurons in the mammalian hypothalamus. *Cell Tissue Res* **375**, 23-39 (2019).
19. Lodato, M.A. *et al.* SOX2 co-occupies distal enhancer elements with distinct POU factors in ESCs and NPCs to specify cell state. *PLoS Genet* **9**, e1003288 (2013).
20. Vierbuchen, T. *et al.* Direct conversion of fibroblasts to functional neurons by defined factors. *Nature* **463**, 1035-1041 (2010).
21. Suva, M.L. *et al.* Reconstructing and reprogramming the tumor-propagating potential of glioblastoma stem-like cells. *Cell* **157**, 580-594 (2014).
22. Zeng, H. *et al.* Bi-allelic Loss of CDKN2A Initiates Melanoma Invasion via BRN2 Activation. *Cancer Cell* **34**, 56-68 e59 (2018).
23. Schlesinger, S. & Meshorer, E. Open Chromatin, Epigenetic Plasticity, and Nuclear Organization in Pluripotency. *Dev Cell* **48**, 135-150 (2019).

24. Fernandez Garcia, M. *et al.* Structural Features of Transcription Factors Associating with Nucleosome Binding. *Mol Cell* **75**, 921-932 e926 (2019).
25. Malik, V., Zimmer, D. & Jauch, R. Diversity among POU transcription factors in chromatin recognition and cell fate reprogramming. *Cell Mol Life Sci* **75**, 1587-1612 (2018).
26. Mu, P. *et al.* SOX2 promotes lineage plasticity and antiandrogen resistance in TP53- and RB1-deficient prostate cancer. *Science* **355**, 84-88 (2017).
27. Ku, S.Y. *et al.* Rb1 and Trp53 cooperate to suppress prostate cancer lineage plasticity, metastasis, and antiandrogen resistance. *Science* **355**, 78-83 (2017).
28. Akamatsu, S. *et al.* The Placental Gene PEG10 Promotes Progression of Neuroendocrine Prostate Cancer. *Cell Rep* **12**, 922-936 (2015).
29. Urban, S. *et al.* A Brn2-Zic1 axis specifies the neuronal fate of retinoic-acid-treated embryonic stem cells. *J Cell Sci* **128**, 2303-2318 (2015).
30. Herbert, K. *et al.* BRN2 suppresses apoptosis, reprograms DNA damage repair, and is associated with a high somatic mutation burden in melanoma. *Genes Dev* **33**, 310-332 (2019).
31. Nuytten, M. *et al.* The transcriptional repressor NIPP1 is an essential player in EZH2-mediated gene silencing. *Oncogene* **27**, 1449-1460 (2008).
32. Layer, R.M. *et al.* GIGGLE: a search engine for large-scale integrated genome analysis. *Nat Methods* **15**, 123-126 (2018).
33. Vignali, M., Hassan, A.H., Neely, K.E. & Workman, J.L. ATP-dependent chromatin-remodeling complexes. *Mol Cell Biol* **20**, 1899-1910 (2000).
34. Muchardt, C. & Yaniv, M. ATP-dependent chromatin remodelling: SWI/SNF and Co. are on the job. *J Mol Biol* **293**, 187-198 (1999).
35. Mashtalir, N. *et al.* Modular Organization and Assembly of SWI/SNF Family Chromatin Remodeling Complexes. *Cell* **175**, 1272-1288 e1220 (2018).
36. Son, E.Y. & Crabtree, G.R. The role of BAF (mSWI/SNF) complexes in mammalian neural development. *Am J Med Genet C Semin Med Genet* **166C**, 333-349 (2014).
37. Chiba, H., Muramatsu, M., Nomoto, A. & Kato, H. Two human homologues of Saccharomyces cerevisiae SWI2/SNF2 and Drosophila brahma are transcriptional coactivators cooperating with the estrogen receptor and the retinoic acid receptor. *Nucleic Acids Res* **22**, 1815-1820 (1994).
38. Clapier, C.R., Iwasa, J., Cairns, B.R. & Peterson, C.L. Mechanisms of action and regulation of ATP-dependent chromatin-remodelling complexes. *Nat Rev Mol Cell Biol* **18**, 407-422 (2017).
39. Khavari, P.A., Peterson, C.L., Tamkun, J.W., Mendel, D.B. & Crabtree, G.R. BRG1 contains a conserved domain of the SWI2/SNF2 family necessary for normal mitotic growth and transcription. *Nature* **366**, 170-174 (1993).
40. Wang, W. *et al.* Purification and biochemical heterogeneity of the mammalian SWI-SNF complex. *EMBO J* **15**, 5370-5382 (1996).
41. Hohmann, A.F. & Vakoc, C.R. A rationale to target the SWI/SNF complex for cancer therapy. *Trends Genet* **30**, 356-363 (2014).
42. Kadoch, C. *et al.* Proteomic and bioinformatic analysis of mammalian SWI/SNF complexes identifies extensive roles in human malignancy. *Nature genetics* **45**, 592-601 (2013).
43. Shain, A.H. & Pollack, J.R. The spectrum of SWI/SNF mutations, ubiquitous in human cancers. *PLoS One* **8**, e55119 (2013).
44. Cyrta, J. *et al.* Role of specialized composition of SWI/SNF complexes in prostate cancer lineage plasticity. *Nat Commun* **11**, 5549 (2020).
45. Prensner, J.R. *et al.* The long noncoding RNA SChLAP1 promotes aggressive prostate cancer and antagonizes the SWI/SNF complex. *Nature genetics* **45**, 1392-1398 (2013).
46. Witkowski, L. *et al.* Germline and somatic SMARCA4 mutations characterize small cell carcinoma of the ovary, hypercalcemic type. *Nature genetics* **46**, 438-443 (2014).
47. Jones, S. *et al.* Frequent mutations of chromatin remodeling gene ARID1A in ovarian clear cell carcinoma. *Science* **330**, 228-231 (2010).
48. Versteege, I. *et al.* Truncating mutations of hSNF5/INI1 in aggressive paediatric cancer. *Nature* **394**, 203-206 (1998).

49. Laurette, P. *et al.* Chromatin remodellers Brg1 and Bptf are required for normal gene expression and progression of oncogenic Braf-driven mouse melanoma. *Cell Death Differ* **27**, 29-43 (2020).
50. Buscarlet, M. *et al.* Essential role of BRG, the ATPase subunit of BAF chromatin remodeling complexes, in leukemia maintenance. *Blood* **123**, 1720-1728 (2014).
51. Kadoch, C. & Crabtree, G.R. Reversible disruption of mSWI/SNF (BAF) complexes by the SS18-SSX oncogenic fusion in synovial sarcoma. *Cell* **153**, 71-85 (2013).
52. Marshall, T.W., Link, K.A., Petre-Draviam, C.E. & Knudsen, K.E. Differential requirement of SWI/SNF for androgen receptor activity. *The Journal of biological chemistry* **278**, 30605-30613 (2003).
53. Link, K.A. *et al.* Targeting the BAF57 SWI/SNF subunit in prostate cancer: a novel platform to control androgen receptor activity. *Cancer Res* **68**, 4551-4558 (2008).
54. Muthuswami, R. *et al.* BRG1 is a prognostic indicator and a potential therapeutic target for prostate cancer. *J Cell Physiol* **234**, 15194-15205 (2019).
55. Ding, Y. *et al.* Chromatin remodeling ATPase BRG1 and PTEN are synthetic lethal in prostate cancer. *J Clin Invest* **129**, 759-773 (2019).
56. Xiao, L. *et al.* Targeting SWI/SNF ATPases in enhancer-addicted prostate cancer. *Nature* **601**, 434-439 (2022).
57. Mohammed, H. *et al.* Rapid immunoprecipitation mass spectrometry of endogenous proteins (RIME) for analysis of chromatin complexes. *Nat Protoc* **11**, 316-326 (2016).
58. Scholtes, C., Dufour, C.R. & Giguere, V. Rapid immunoprecipitation mass spectrometry of endogenous protein (RIME) to identify chromatin-interactome in prostate cancer cells. *STAR Protoc* **3**, 101434 (2022).
59. Kondili, M. *et al.* UROPA: a tool for Universal RObust Peak Annotation. *Sci Rep* **7**, 2593 (2017).
60. Abida, W. *et al.* Genomic correlates of clinical outcome in advanced prostate cancer. *Proc Natl Acad Sci U S A* **116**, 11428-11436 (2019).
61. Beltran, H. *et al.* Divergent clonal evolution of castration-resistant neuroendocrine prostate cancer. *Nat Med* **22**, 298-305 (2016).
62. Zhang, Y. *et al.* Model-based analysis of ChIP-Seq (MACS). *Genome Biol* **9**, R137 (2008).
63. Persad, S. *et al.* SEACells infers transcriptional and epigenomic cellular states from single-cell genomics data. *Nat Biotechnol* (2023).
64. Linder, S. *et al.* Drug-Induced Epigenomic Plasticity Reprograms Circadian Rhythm Regulation to Drive Prostate Cancer toward Androgen Independence. *Cancer Discov* **12**, 2074-2097 (2022).